Scope of the Conference

The International Conference on Science and Technology of Complex Fluids (ICSTCF) has a very important tradition in México, and has been organized with the main idea of gathering scientist interested in topics related to soft condensed matter. This conference has also intended to encourage the participation of young undergraduate and graduate students. The scientific focus of the conference is on timely and relevant topics of the science and technology of complex fluids. Particular emphasis is given to novel methods and tools of experimental research, numerical simulation, and theory in complex fluids and soft matter research fields. The aim of the conference is to stimulate collaborations among members of the international scientific and technological community and industry.

The conference consists on lectures, a series of short talks and posters presented by the attendees. In view of the circumstances of the COVID-19 pandemic, the 33rd International Conference on Science and Technology of Complex Fluids has been held online on October 25-28, 2021, at the Universidad de Guanajuato, Sede Forum, León, Guanajuato, México, via the platform Zoom, whereas the posters have been presented via Twitter:

http://www.dci.ugto.mx/~icstcf/index.php/postersession

There is also a link in the web page of the conference where the invited lectures are publicly available:

http://www.dci.ugto.mx/~icstcf/index.php

We appreciate a lot the enthusiast participation of all speakers and attendees in our conference, and we hope to see you again in the 2022 edition, which we foresee it will be presencial in Mexico.

The organizers of the 33rd International Conference on Science and Technology of Complex Fluids.

Invited Talks 1

Posters 30

Active carpets: Learning to transport at the microscale

Dr. Francisca Guzmán-Lastra

Facultad de Estudios Interdisciplinarios, Universidad Mayor de Chile, Chile

Abstract

Active matter is a discipline that lives on the core between physics and biology, in it we try to describe the behavior of living organisms and the way they interact through equations that reproduce their movement.This kind of life is abundant when we look under the microscope. Microorganisms are particularly active and abundant on surfaces, from the cilia in the airway borne to biofilms made up of bacteria. In this trip we will discover how this activity on surfaces is capable of transporting molecules and self-cleaning when they are not self-organized and how they are capable of feeding themselves when they move collectively.

Thermally activated transitions of a Brownian particle in a viscoelastic fluid environment

Dr. Juan Ruben Gomez Solano

Instituto de Física, Universidad Nacional Autónoma de México, México

Abstract

Thermally activated transitions are ubiquitous in nature, such as in chemical reactions, protein folding, and drug binding, to name but a few. Although this phenomenon is nowadays well understood when occurring in perfectly viscous environments, very little is known about thermally-activated transitions in viscoelastic fluids. This kind of non-Newtonian materials with intricate flow properties, e.g., polymer solutions, micellar fluids, and colloidal suspensions, are widespread in many soft matter systems of greatest relevance to both fundamental and applied sciences. In this work, we investigate the motion of a micron-sized bead embedded in a micellar viscoelastic fluid transiting between the wells of a bistable optical potential. The precise characterization of both the potential and the fluid viscoelasticity enables a neat comparison between our experimental results and a theoretical model based on the generalized Langevin equation.

Our findings reveal an amplification of the transition rates, as compared o those in a Newtonian fluid, which stems from the interplay between the slow relaxation of fluid and the nonequilibrium particle dynamics around the potential barrier. Our analysis provides a general understanding of the effect of viscoelastic memory friction on the escape of a Brownian particle from a metastable state, which is a prerequisite for further investigations on transport phenomena in more complex energy landscapes and environments, as those commonly encountered in many biological processes and mesoscopic controlled delivery systems.

The complex and fascinated world of the paints. How to understand it using innovation and collaboration

Dr. Isabel Sáenz de Buruaga Yurramendi

R&D Director, Centro de Investigación en Polímeros, PPG Comex, México

Abstract

In this presentation I will introduce the complexity of the paints and some of the technologies that we use to understand the phenomena that occur in these systems. I will talk about rheology, the influence of the characteristics of the polymer particles and pigments in the final properties and the interactions between the different components and additives. At the same time, I will introduce the innovation methodology that we use in our Company, and the way we work in collaboration with Universities and external Institutions.

Applied Physics: connecting physics and engineering for practical purposes

Dr. Carmen Lucía Moraila Martínez

División de Ciencias e Ingenierías, Universidad de Guanajuato, México

Abstract

Applied Physics is a generic term used to describe the part of physics that is particularly interested in the use of technologies to solve practical problems.

In this talk I will present the results obtained in some of our projects in different areas such as medicine and engineering. I will talk about the role of red blood cells electrical charge to diagnose diseases as a low resource technique. I will present the results obtained of erythrocytes Zeta Potential measurements of patients with different states of health. At the same time, I will introduce the study of promising graphene-derived materials, such as graphene oxide, reduced-graphene oxide and laser-induced graphene, for their use in flexible electronics devices for biomedical applications.

Foams with viscoelastic continuous phases: changing foam coarsening with an emulsion

Dr. Anniina Salonen

Laboratoire de Physique des Solides, Université Paris-Saclay, France

Abstract

Foams are gas bubbles in a continuous phase. They are metastable and disappear in time unless the ageing processes are stopped for example by solidifying the continuous phase, to make solid foams. However, we do not always want solid foams, just more stable "liquid foams". The challenge is to understand, and thus control, the ageing processes.

One way to change foam stability is by changing the mechanical properties of the continuous phase using a viscoelastic fluid, such as emulsion, colloidal gel, polymer etc. Indeed foams from viscoelastic fluids can be much more stable, slowing down the three ageing processes of coarsening, coalescence and drainage. Many common foamed materials have viscoelastic continuous phases, such as whipped cream or foamed cement. We work with foamed emulsions. We use oil in water emulsions as the continuous phase, because this allows us to control the emulsion mechanical properties through changing oil volume fraction and drop interactions. We focus on the coarsening of pseudo-2D foams to avoid drainage, and to allow us to follow the foam structure in time.

We show that the elasticity of the continuous phase strongly influences the ripening of foamed emulsions, leading to reduced bubble growth rates. Moreover, we show that emulsion viscoelasticity also affects the foam structure, with the appearance of unrelaxed bubble patterns. The results can lead to a more efficient control of the foam structure and stability.

Polymers Bio-Conjugates: an in silico Perspective

Dr. Coray Colina

Department of Chemistry, University of Florida, USA

Abstract

Biology has perfected the molecular connection between form and function that synthetic chemists can only dream of. Remarkable advances have used biomimetics to create novel multifunctional materials, but there remains a chasm of science that prevents the seamless fusion of the biotic and abiotic worlds. Bioconjugates (i.e., biologically-inspired molecular hybrids consisting of synthetic and biomacromolecular components such as proteins) offer the promise of deploying the exquisite selectivity and functionality of biology across a broad range of fields. Ultimately, computational science offers considerable potential to move beyond the current state-of-the-art in rational design strategies. Molecular dynamics simulations have traditionally been used to study the dynamics of native protein structure at both the all-atom and coarse-grain level of detail and can be designed to mimic experimental conditions. Our challenge is to predict in silico the dependence of bioconjugates solubility and dynamics on polymer length, chemistry, and density. In this talk I will highlight the fundamental tools to simulate how polymers impact protein dynamics. Examples will be shown of how this approach enabled the sampling and understanding of many tunable characteristics of the conjugated polymers (e.g., polymer length, chemistry, attachment site, and grafting density).

Tannins as green micro-mesoporous carbon precursors for a wide range of environmental and energy applications

Dr. Vanessa Fierro

CNRS Research Professor at Institut Jean Lamour, France

Abstract

Tannins are naturally occurring polyphenolic molecules that have a number of unique advantages: they are bio-based, commercially available at low cost, reproducible, non-toxic but reactive. These precursors are the natural counterpart of resorcinol and phenol, from which many carbon materials have been described. They can even polymerise without a cross-linker by self-condensation, leading to formaldehyde-free carbon precursors for example. The exceptional richness of possible formulations also makes it possible to produce thermosetting resins of all morphologies, which, once polymerised, are insoluble and infusible and thus make it possible to obtain carbonaceous materials with a totally controlled structure.

Tannin-derived carbons can be partly graphitized, and so that the entire series of nanotextures from vitreous carbon to graphite-like through turbostratic carbon can be obtained. Thus, not only are the most diverse structures possible through adequate structuring of the precursor resins, but also once the carbons have been obtained, the performances are up to expectations, whether they concern electrochemistry or adsorption for example. This can be explained by the possibility of adjusting the texture of the carbon, but also by the fact that the carbon obtained is reactive and therefore responds very well to doping and surface functionalisation, further extending its already very wide range of uses.

In this talk, I will show that there are a multitude of applications for which these tannin-derived micro-mesoporous carbons can be successfully used. Supercapacitor electrodes, carbon molecular sieves, platinum-free electrocatalysts for the oxygen reduction reaction in PEMFC fuel cells, adsorption of CO_2, water/hydrocarbon separation, amongst others.

Engineering fluid-fluid interfaces through processing and multicomponent adsorption

Dr. Lynn Walker

Department of Chemical Engineering, Carnegie Mellon University, USA

Abstract

Systems involving deformable interfaces between immiscible fluids offer a significant challenge for materials design and processing. Static interfacial/surface tension is often the only parameter considered in the design of systems with fluid-fluid interfaces. In foams, emulsions, blends, sprays, droplet-based microfluidic devices and many other applications, the dynamic nature of surface active species and deformation of interfaces requires a more detailed characterization of the interfacial transport, dynamic interfacial properties and interfacial structure. Macroscopic properties and the ability to tune and control phenomena requires an improved understanding of the time-dependent properties of the interfacial tension and interfacial mechanics. We have developed tools and approaches to quantify the impact of surface active species on interfacial behavior. Surfactant-nanoparticle complexes, polymer-surfactant aggregates and proteins show the potential of interfacial processing in controlling interfacial properties. The use of sequential adsorption, differences in transport timescales and variability in reversibility of different species allows interfaces to be engineered. This talk will provide the motivation to use microscale interfaces for efficient analysis of complex interfacial phenomena and how that relates to the material properties of interface-dominated materials.

Viscoelastic fluids through porous media: flow instability and particle transport

Dr. Arezoo M. Ardekani

Department of Mechanical Engineering, Purdue University, USA

Abstract

Viscoelastic fluid flows through porous media are common in industrial and biological applications ranging from oil recovery and groundwater remediation to drug transport in tissue. Polymeric stresses affect the topology and stability of these flows, and thus, their macroscopic transport properties. We numerically study the flow topology, instability, and dispersion of viscoelastic flow through porous media. Inertial stresses here are negligible, and instead, the flow is dominated by elasticity and viscosity; their relative effects are characterized by the Weissenberg number. At small Weissenberg numbers, stable eddies appear, whereas at large Weissenberg numbers, strong flow fluctuations due to high polymeric stresses lead to the formation of highly unstable eddies in different regions of the pores and multiple distinct unstable flow structures occur. The stretched polymeric chains inside the pore facilitate eddy formation, whereas relaxed chains lead to eddy free regions. We also discuss the dispersion of particles in these flows.

Solid-state nanopores as biomimetic signal-transducing nanosystems:

Nature as a source of inspiration for engineering nanofluidic devices

Dr. Omar Azzaroni

Instituto de Investigaciones Fisicoquímicas Teóricas y Aplicadas, Universidad Nacional de La Plata, Argentina

Abstract

Much of the inspiration to construct highly functional architectures comes from the millennial quest of man to look at nature's complete technological design. Biological structures provide a wide range of systems with different functions that ultimately serve as a source of inspiration in materials science. In this way, biomimetic materials research facilitated numerous avenues to create multifunctional materials by blending concepts from different disciplines. For instance, as we move further into the new century, the convergence of chemistry, physics and nanotechnology seems indeed to offer almost unlimited opportunities for constructing biomimetic nanosystems and devices via top-down and bottom-up approaches. In all living systems biological channels work as nanodevices in charge of regulating key functions such as electric potential, ionic flow, and molecular transport across the boundaries of the cells. Along these lines, the virtues of working with nanofluidic elements are being increasingly recognized by the biomimetics research community. This has led to the emergence of a research area that is currently at the forefront of materials science and engineering. The advent of track-etching techniques ("top-down approach") has resulted in an increasing mastery in construction of nanoscale fluidic structures and has given a decisive impetus not only to the development of this exciting area of nanotechnology but also opened up new possibilities to reproducibly engineer nanopore and nanochannel architectures with various shapes and diameters down to a few nanometers. This endeavor gave rise to design concepts to construct fully "abiotic" nanochannels with dimensions comparable to those of biological molecules. One major attraction of these nanofluidic elements is their outstanding ability to control and manipulate the transport of chemical and biochemical species flowing through them, thus enabling the construction of ionic circuits capable of sensing, switching, or separating diverse species in aqueous solutions. Furthermore, these nanofluidic devices have also been shown to display transport properties that resemble biological protein ion channels, such as ion selectivity, current rectification, flux inhibition by protons and divalent cations, transport of ions against concentration gradients, and even ion current fluctuations. In the particular case of asymmetric nanochannels/nanopores, appealing rectification effects arise when the channel surface is charged and the dimensions are comparable to the Debye length. These fascinating physicochemical properties displayed by charged nanochannels or nanopores provided the scenario to create new functional and addressable nanofluidic architectures and also led to the birth of a whole new area of research concerning the design of nanochannel-based devices resting on surface charge governed ionic transport. However, in order to confer selectivity to solid-state nanopores, it is necessary to develop and explore new methods for functionalizing the pore walls. Hence, the creation of functional nanopores capable of acting as selective ion channels or smart nanofluidic sensors depends critically on our ability to assemble and build up molecular architectures in a predictable manner within confined geometries with dimensions comparable to the size of the building blocks themselves. In this context, we have been working to integrate macro- and supramolecular assemblies into track-etched solid state nanopores in order to create chemical nanodevices displaying a wide variety of functional features. We seek to further the rich interplay between the complexity and versatility of "soft" building blocks and the remarkable physical characteristics of solid-state nanopores. We consider that these results can lead to a new way of looking at interdisciplinary research in biomimetic materials science and trigger a cascade of new, refreshing ideas in nanochemistry aimed at the rational design of functional biomimetic assemblies with unprecedented properties.

Ion transport and chemical reactions in nanoporous materials for environmental engineering

Dr. Jouke Dykstra

Environmental Technology, Wageningen University, The Netherlands

Abstract

In my presentation I will illustrate the theory focussing on two processes: I) an electrochemical separation process for the removal of boron, a toxic ion, from water, and II) a(n) (bio)electrochemical process for the production of acetate from CO2.

In the first process, electrochemical separation for the removal of boron from water, porous carbon electrodes are employed for the electrosorption of boron from water. Several processes must be described. Firstly, the transport of ions due to advection, diffusion and migration must be included. Secondly, the electrosorption of ions in electrical double layers formed in porous carbon electrodes must be described. Thirdly, in these double layers chemical phenomena, such as the binding of protons to surface groups, must be considered. Lastly, acid-base equilibria must be included. I will present a theoretical description of these joint processes and I will show how this description can contribute to the development of an effective process to remove amphoteric ions, including boron, from water.

In the second process, electrochemical cells are applied that rely, for the production of acetate, on conductive biofilms covering an electrode. I will show how we can derive a theoretical model to describe the transport of amphoteric ions and electrons, coupled to biochemical conversions, through a current-producing biofilm. This theoretical approach can be extended and can be employed to describe ion transport, interfacial phenomena (faradaic and non-faradaic processes), and chemical reactions in other (porous) media as well.

Investigation of Thermoelectric Semiconductors with Electric Double Layer Gating

Dr. Sunao Shimizu

Central Research Institute of Electric Power Industry (CRIEPI), Japan

Abstract

Thermoelectric energy conversion has recently regained an increased interest as a promising technology for generation of renewable energy. It is highly required to develop novel thermoelectric materials from diverse library of functional materials. For exploring thermoelectric semiconductors, we have applied an ionic liquid gating technique as a tool to systematically control the carrier density. Due to the high gate capacitance at the electric double layer, high density charge carriers are accumulated on the semiconductor surface by just applying several volts of the gate voltage. The highest carrier density reaches up to 10 14 ~ 10 15 cm - 2 , which covers insulating to metallic region of inorganic materials.

In this presentation, we would like to report our recent studies on thermoelectric materials investigated by electric double layer transistor (EDLT) configurations. We will present how the thermoelectric effect is modulated by liquid gating and would like to discuss their properties unique to their intrinsic band structures. Our approach is applicable to wide range of materials, opening up a novel route to realize thermoelectric devices with advanced functionalities.

Electronic transport properties of graphene-polymer nanocomposites

Dr. Roxana Mitzayé Del Castillo Vazquez

Departamento de Física, Facultad de Ciencias, Universidad Nacional Autónoma de México, México

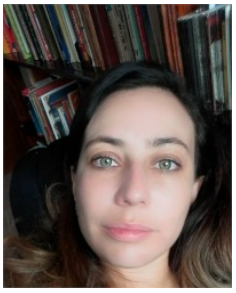

Abstract

It has been studied the electronic properties of compounds formed by graphene and polymers. The study makes a comparative analysis between experimental and computational results. To make an experimental measurement of the electronic properties, we deposited graphene nanoparticles over a polypropylene matrix. The deposition was made in several stages. We added different percentages of graphene nanoparticles to the polymer matrix using the melt compounding technique, and we studied microwave adsorption. The experimental conductivity was measured using electrochemical spectroscopy impedance equipment. The second part consists of computational calculations, in which we studied the electronic properties of a graphene sheet under one polypropylene molecule with different degrees of polymerization. We observed a strong percolation phenomenon with a percolation threshold of around 18% of MLG nanoparticles. Before the percolation threshold, the charge carriers are constrained in the polypropylene molecule, making the system an insulating material. After the percolation threshold, the charge carriers are constrained in the graphene, making the system a conductor material. Incorporating the quantum effects and the percolation phenomenon makes it possible for the theoretical conductivity to be close to the experimental conductivity.

To extrapolate our research to several polymers systems with graphene, we have made a stochastic study of the problem to observe how the phenomenon of percolation on different graphene-polymer nanocomposites. We simulate the deposition and transport phenomena with a Monte-Carlo simulation. We compared our results with the experimental studies, and we obtained a reasonable estimation of the percolation threshold and the observed conductivity.

Angle-dependent physical properties of 2D van der Waals heterostructures

Dr. Cecilia Noguez

Instituto de Física, Universidad Nacional Autonoma de México, México

Abstract

Until now, much has been done to study, theoretically and experimentally, the physical properties of two vertically stacked G layers with a different crystallographic orientation between them characterized by an angle. This angle between layers emerges as a new degree of freedom, which specifies physical properties such as electronic, optical, chemical, among others. Some exciting experimental results have been found very recently in these superlattices, but deep theoretical understanding has been lagged. One of the reasons is that typical electronic structure analysis methods are insufficient. In particular, band structures get crowded because of Brillouin Zone folding, making their interpretation cumbersome. In this talk, we present a methodology that allows us to elucidate the physical effects of the mutual interactions between 2D layers by unfolding the electronic bands of systems with double periodicity. This method reveals that new gaps that turn into discrete-like states evenly-spaced in energy arise and are modulated when the interlayer angle decreases. These electronic states might be relevant to explain, for instance, electron-phonon assisted effects recently observed in experiments.

Towards understanding the mechanism of formation of porous silicate crystals

Dr. Valeria Molinero

Professor of Theoretical Chemistry, The University of Utah, USA

Abstract

Zeolites are porous silicates that constitute the main solid catalysts used by the chemical industry. These structurally complex solids are synthesized from aqueous solutions through a multi-stage process that involves multiple phase transitions mediated by the chemistry of polymerization of silica. Organic cations, typically tetraalkylammonium ions, are used to direct the synthesis towards specific zeolite polymorphs. Nevertheless, the molecular mechanisms by which the cations and silicates form the zeolites are not well understood. This presentation will discuss our current work using molecular simulations with simple models to elucidate these mechanisms and understand whether metastable mesophases could be involved in the nucleation mechanism, at which stage the pores and zeolitic order develop, and what is the smallest size of nanozeolite that can be synthesized.

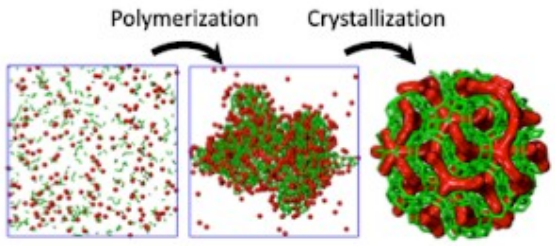

Collective Dynamics of Self-Propelled Camphor Rotors

Jyoti Sharma[1], Ishant Tiwari[1], Véronique Pimienta[2], V.S Akella[3], Dibyendu Das[1], Punit Parmananda[1]

[1]Department of Physics, IIT Bombay, Mumbai, India
Email: jyoti_sharma@iitb.ac.in

[2] Laboratoire des IMRCP, Université de Toulouse, Toulouse, France

[3] Department of Physics, IIT Jammu, Jammu & Kashmir, India

Abstract

The collective dynamics of self-propelled entities has recently attracted much attention. Easy to set up experimental systems exploring the artificial self-moving particles hold potential in understanding self-propulsion in biological entities. I will present tabletop experiments on a well known camphor system [1]. Our experiment incorporates a self-propelled camphor rotor as an oscillator. Camphor rotor/ribbon is a rectangular piece of paper with camphor infused in its' matrix. It exhibits self-motion on the water surface due to the surface tension imbalance around it. Two such pinned camphor rotors showed synchronized dynamics at the air-water interface[2]. Following this, ensemble dynamics of three, four, and five rotors were studied. In different geometries, again synchronized configurations were observed [3]. Furthermore, I will show experiments on three globally coupled camphor rotors revealing peculiar states known as chimera like states[4]. We characterize chimera like states by the coexistence of one synchronized and two unsynchronized ribbon pairs. We rationalize the mechanism of collective rotational dynamics of camphor ribbons via a numerical model incorporating Yukawa potential.

References

[1] Nakata Satoshi, Iguchi Yasutaka, Ose Sachie, Kuboyama Makiko, Ishii Toshio and Yoshikawa Kenichi, "Self-rotation of a camphor scraping on water: New insight into the old problem" **Langmuir, 13, 16, 4454-4458 (1997).**

[2] Sharma Jyoti, Tiwari Ishant, Das Dibyendu, Parmananda P, Akella V.S, and PimientaVeronique,"Rotational synchronization of camphor ribbons" **Phys. Rev. E 99, 012204 (2019).**

[3] Sharma Jyoti, Tiwari Ishant, Das Dibyendu, Parmananda P. and Pimienta Veronique,"Rotational synchronization of camphor ribbons in different geometries" **Phys. Rev. E 101, 052202 (2020).**

[4] Sharma Jyoti, Tiwari Ishant, Das Dibyendu and Parmananda P, "Chimera like states in a minimal network of active camphor ribbons" **Phys. Rev. E 103, 012214 (2021).**

Directed self-assembly of polymerizable blue-phase liquid crystals

Tadej Emeršič[1]*, Kushal Bagchi[1], José A. Martínez-González[2], Xiao Li[3], Paul F. Nealey[1,4], Juan J. de Pablo[1,4]

[1] *Pritzker School of Molecular Engineering, The University of Chicago*
5640 South Ellis Avenue, Chicago, IL 60637
emersic@uchicago.edu, kbagchi@uchicago.edu

[2] *Facultad de Ciencias, Universidad Autónoma de San Luis Potosí*
Av. Parque Chapultepec 1570, 78210 San Luis, S.L.P., Mexico
jose.adrian.martinez@uaslp.mx

[3] *Department of Materials Science and Engineering, University of North Texas*
University of North Texas Discovery Park, 3940 N Elm St, Denton, TX 76207
xiao.li@unt.edu

[4] *Center for Molecular Engineering, Argonne National Laboratory*
9700 S Cass Ave, Lemont, IL 60439
nealey@uchicago.edu, depablo@uchicago.edu

Abstract

Blue-phases (BPs) occur in chiral liquid crystals in a narrow temperature window between the chiral nematic and the isotropic phases. BPs exhibit unit cell sizes of the order of 100's nm, making them soft photonic crystals. Possessing unique structural and optical properties, they have been regarded as one of the most promising candidates for applications in displays, sensors, and lasing. However, polycrystallinity and thermal instability of BPs have still greatly limited their applicability. Chemically patterned surfaces with alternating planar and homeotropic anchoring regions can be used for the epitaxial growth of monocrystalline BPs with a prescribed lattice orientation. In this work, we show that such a simple stripe-like pattern symmetry with different interfacial energy can direct the self-assembly of BP forming mixtures with different chemical compositions into monocrystals. Our experiments together with the support of free energy theoretical calculations propose that the strategy of nano-patterned substrates is generally applicable and may serve as a general platform for nucleation and growth of stable, macroscopic single crystalline area with controlled crystal orientation. Each large single monocrystal of selected BP liquid crystal mixtures reflects the light differently which results in the formation of a colorful spectrum of monocrystals. Moreover, our experiments also demonstrate that the thermal stability of such prepared monocrystals can be dramatically improved by photopolymerization, which freezes and retains the BP structure. This indicates that combining the directed self-assembly and the photopolymerization methods lead to the preparation of thermally stable BP monocrystals of a desire lattice orientation. Engineering and controlling the lattice orientation of the polymerized monocrystals greatly improves the applicability of BPs for technological applications.

Keywords: blue-phase liquid crystals, chemical patterns, directed self-assembly, monocrystals, photopolymerization

Elliptical Chemoreceptors: The key to an Effective Absorption

Jason B. Peña[1] **and Leonardo Dagdug**[1,2]

[1]*Metropolitan Autonomous University at Iztapalapa*
Av. San Rafael Atlixco 186, Leyes de Reforma 1ra Secc, Iztapalapa, 09340 Ciudad de México, México
jason.penmunoz@gmail.com

[2]*National Institutes of Health, Shriver National Institute of Child Health and Human Development*
29 Lincoln Drive, Building 29B, Bethesda, MD 20892, U.S.
dll@xanum.uam.mx

Abstract

Models of molecules transport through diffusion offer an important insight into the description of microscopic phenomena in nature. In the research, we focused on some models of chemoreception, from the perfect spherical absorbent, the use of Weber's disk, and the development of Berg and Purcell approach, to Zwanzig and Szabo generalized solution where interference effect and partially absorbing receptors are considered. Afterwards, we extrapolate Dudko's solution using a dimensional comparison for rate constant diffusion to receptors of arbitrary shape on a spherical cell, and contrast the absorption effectiveness on circular and elliptical chemoreceptors, using as reference the perfect spherical absorbent. During this process we looked to an important property related with the structure of chemoreceptors, their geometry. Is there a preferential setting that allows more particles to be absorbed in an ever smaller area? We found that the elliptical geometry offers a plausible model in cellular anatomy, a result that could explain the structure variation on chemoreceptors and the observed physiological changes on cells.

Keywords: Cells, membranes, diffusion, biological models, biophysics, chemoreceptors.

1. Introduction

It is well known that cells are a fundamental part in the existence of life, a little organic machine capable of making big things, thanks to which we can breathe, move and reproduce. Not mentioning, that cells are responsible of the embryogenesis process. In addition to the existentiality of cells it is necessary that they work correctly, and most of the times, that depends on the cellular intercommunication, a mechanism that can be reduced into three steps; the reception, transduction and response. By the scope of the research we concentrate on the first step, the reception of signaling molecules or ligands. These particles carry useful information to the cells causing them to migrate, reproduce, or even die. A schematic representation of the cellular intercommunication is shown in Fig. 1.

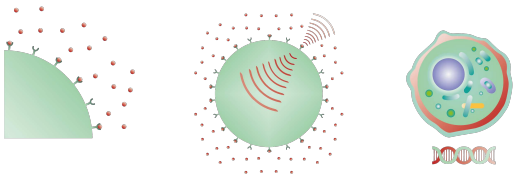

Figure 1: Schematic representation of the intercellular information exchange sequence. From left to right, receptor-ligand interaction, transduction (amplification of molecular signals) and specific physiological response, DNA transcription in the cell nucleus are represented.

Guided by chemical reactions, cells are a complex system that create and dismantle structures, besides making perfect copies of themselves. This biochemical network could go wrong when tiny mistakes add up until the machinery gets corrupted, something that could lead into biological disorders, like cancer. Intercellular communication is as important as the existence of cells, and the interaction receptor-ligand is the very first part of this process, a phenomenon that can be modeled with diffusion equations.

2. A counter-intuitive mental experiment

Before diving into the research details we set a mental experiment related with the absorption of particles. Suppose we have two spheres, one of which has one reflective and one absorbent hemisphere, while the second has tiny, uniformly distributed absorbent circular patches on the surface, so that together, occupy a minimal area on the cell membrane, say 6 thousandths of it. The question is: Which configuration can absorb more molecules if they are immersed in a fluid with an specific concentration gradient?

The answer seems to be obvious, as the first sphere has a much larger absorbent total area than the second one. In 1977, Berg and Purcell gave a counter-intuitive solution to this chemoreception problem [1], The two configurations can absorb exactly the same!

3. Evolution of a model

The chemoreception model has been modified through the years [3,4,5], in order to approximate it to reality as much as possible, like the Zwanzig modification, in the interference effect [4], and the introduction of patches with selectivity information by Zwanzig and Szabo [5]. The latter being

$$\frac{1}{k_{ZS}} = \frac{1}{k_S} + \frac{(1-\sigma)}{Nk_H} + \frac{1}{Nk\pi s^2} \tag{1}$$

A result derived from the use of the Smoluchowski constant,

$k_S = 4\pi Da$, associated with the perfect spherical absorbent, and the Hill constant, $k_H = 4Ds$, which comes from the Weber's disk; where a and s are the radii of the sphere and of the receptors, respectively and D is the diffusion coefficient, which is considered to be constant. On the other hand, σ is the occupied area by the patches, N the number of receptors and k the permeability of the system. It's important to mention that we are interested in the constant current diffusion because it will tell us the number of particles absorbed per unit time, a perfect parameter to measure the nutrition of the cell. Circular patches were used in all of the modifications, but, does the geometry of the receptors have a considerable effect on the absorption capacity? A theoretical formulation of non-circular receptors is necessary.

4. The importance of geometry

During the investigation, the diffusion current constant associated with an arbitrarily shaped patch on a reflecting plane, k_G, was calculated, through a comparison between the analytically calculated constant for an elliptical receptor in terms of the eccentricity ϵ and the semi-major axis a_1

$$k_\epsilon = \frac{2\pi D a_1}{k_\epsilon(\epsilon)}, \qquad k_\epsilon(\epsilon) = \int \frac{d\theta}{\sqrt{1-\epsilon^2\sin^2\theta}} \tag{2}$$

in contrast to a purely geometric formulation, which is correctly reduced to circular patches when the area A and perimeter P are given, namely

$$k_{GP} = \frac{2^{1+2\nu}}{\pi^{1-\nu}} A^\nu P^{1-2} \tag{3}$$

A quantity that depends on a numerical parameter ν. By doing this comparison it is found that

$$k_G = \left(\frac{2^5 AP}{\pi^2}\right)^{1/3} D \tag{4}$$

a result that matches with what is reported by Dudko Et al. [2]. After extrapolate the results, the constant current diffusion associated to N patches of area A_R on a spherical surface is

$$\frac{1}{k_{AS}} = \frac{1}{k_S} + \frac{(1-\sigma)}{Nk_G} + \frac{1}{NkA_R} \tag{5}$$

When the interference effect is neglected, the Eqn (5) becomes

$$\frac{1}{k_{PD}} = \frac{1}{k_S} + \frac{1}{Nkk_G} \tag{6}$$

Circular, square, triangular, hexagonal, n-sided polygons, and elliptical patches were treated, all on a reflecting spherical surface. Each showed less effectiveness compared to the circular patches, except the elliptical ones. When using receptors with a permeability of 50%, the number of patches needed to reach the absorbing hemisphere is $N_c = 31,416$, for circular receptors and $N_\epsilon = 31,337$, for elliptical receptors. Where we set the semi-minor axis equals the radius of the circle and $\epsilon = 0.1$. In this way, elliptical receivers take up only 0.25% more space relative to circular ones.

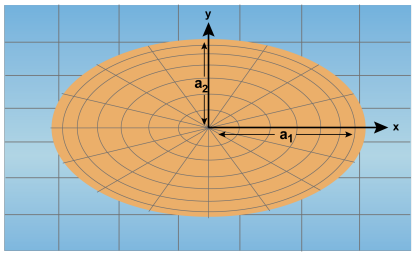

Figure 2: Elliptical chemoreceptor with semi-major axis a_1, semi-minor axis a_2 and eccentricity ϵ on a reflective surface.

The space-absorption ratio is good, but this can be attributed to the fact that an ellipse with this configuration actually has more area than a circle and would ultimately take up more space on the membrane. Nevertheless, when fixing the individual area of the receptors, that is, the area of the circle equal to that of the ellipse and making a relationship between the current constants, the following expression is found

$$\frac{k_{G\epsilon}}{k_{Gc}} = \left[\frac{1-\frac{\epsilon^2}{4}-\frac{3}{64}\epsilon^4}{(1-\epsilon^2)^{1/4}}\right]^{1/3} \tag{7}$$

where $k_{G\epsilon}$ is that of elliptical receptors and k_{Gc} of the circular ones. This number is always greater than one, $k_{G\epsilon} > k_{Gc}\ \forall\ \epsilon > 0$, the absorption capacity is greater if an elliptical geometry is considered, they occupy the same amount of area on the plane but can absorb more signaling molecules.

5. Conclusions

A chemoreceptor distribution is as good as a perfect absorbent hemisphere and it can be better if elliptical receptors are considered. Furthermore, the most effective geometry will be the one with the largest perimeter once the area has been set. It is necessary to recognize the importance of geometry in cellular intercommunication, which could have great applications in bioengineering. Meanwhile, this result is left as an irrefutable improvement to the Berg and Purcell model. Elliptical membrane receptors, the key to effective absorption.

References

[1] Berg, H. C. and Purcell, E. M. Physics of chemoreception. *Biophysical Journal*, 20(2), pp. 193-219, 1977.

[2] Dudko, O.k., Berezhkovskii, A. M. and Weiss, G. H. Rate constant for diffusion-influenced ligand binding to receptors of arbitrary shape on a cell surface. *The Journal of Chemical Physics*, 121(3), pp. 1562-1565, 2004.

[3] Shoup, D. and Szabo, A. Role of diffusion in ligand binding to macromolecules and cell-bound receptors. *Biophysical Journal*,40(1), pp. 33-39, 1982.

[4] Zwanzig, R. Diffusion-controlled ligand binding to spheres partially covered by receptors: an effective medium treatment. *Proceedings of the National Academy of Sciences*, 87(15), pp. 5856–5857, 1990.

[5] Zwanzig, R. & Szabo, A.Time dependent rate diffusion-influenced ligand binding to receptors on cell surfaces. *Biophysical journal*, 60(3), pp. 671-678, 1991.

Hydrophobic-Solute Encapsulation by Amphiphilic Mikto-Grafted Bottlebrushes

Carlos A. Salinas-Soto[1,2] and Abelardo Ramirez-Hernandez[1,2]

[1] *Department of Biomedical Engineering and Chemical Engineering, The University of Texas at San Antonio, San Antonio, Texas 78249, USA*

[2] *Department of Physics and Astronomy, The University of Texas at San Antonio, San Antonio, Texas 78249, USA*

Abstract

Amphiphilic mikto-grafted bottlebrushes offer a wide range of applications in many areas of science and technology due to their self-assembly behavior in the presence of selective solvents. In aqueous solutions, bottlebrushes self-assemble into a variety of nanostructures, including spherical, cylindrical and toroidal micelles as well as vesicles. Interestingly, some of these structures can be formed at very low concentrations given place to unimolecular micelles. These micelles can be loaded with different drugs, thus acting as a drug carrier system, with many potential pharmaceutical applications. For this reason, it is important to understand the self-assembly dynamics and properties of empty and drug loaded micelles in aqueous solutions to improve their performance. In this work, we have performed extensive numerical simulations to elucidate the role of side chain size-asymmetry and bottlebrush molecular weight on the morphology of unimolecular micelles in aqueous solutions. When hydrophobic drugs are incorporated into the solution, these are encapsulated into the polymer structures, and at high enough drug concentration, these solutes are able to induce a shape transition from cylindrical to spherical micelles, as observed in experiments. Our studies focused on two different macromolecules: poly(glycidyl methacrylate)-g-poly(ethylene glycol)/poly(lactic acid) PGMA-g-PEG/PLA and poly(glycidyl methacrylate)-g-Poly(ethylene glycol)/Poly(styrene) PGMA-g-PEG/PS; we modeled doxorubicin (DOX), a cancer treatment drug, as the hydrophobic solute.

*Footnotes may appear on the first page only to indicate research grant, sponsoring agency, etc. These should not be numbered but referred to by symbols, e.g. *,+. The footnote text may be produced in a small font.

On the effect of morphology and particle-wall interaction on colloidal near-wall dynamics

J.A. Rivera-Morán [1], Y. Liu [1], S. Monter [1,2], C.-P. Hsu [3], P. Ruckdeschel [4], M. Retsch [4], M. Lisicki [5] & P.R. Lang [1]

[1] *Forschungszentrum Jülich GmbH, Biomacromolecular Systems and Processes IBI-4*
Leo-Brandt-Straße, 52428 Jülich, Germany
j.rivera.moran@fz-juelich.de; p.lang@fz-juelich.de

[2] *Universität Konstanz, Germany*

[3] *Technische Universität München, Germany*

[4] *Universität Bayreuth, Germany*

[5] *University Warsaw, Poland*

Abstract

In this work, we present how the surface shape of three different types of colloidal particles, in solution, could affect their particle-wall static interaction and thus, how could influence their parallel diffusion coefficient near a glass wall. By using the evanescent wave dynamic light scattering technique, the experimental information is acquired. The particles with a rough surface parallelly diffuse slower than the particles with a smooth surface when they are close to a hard wall. According to hydrodynamic arguments on rough particles and porous-shell particles, these are expected to diffuse faster than the hard-sphere case. To address this, we implemented numerical calculations taking into account both hydrodynamic and static particle-wall interactions. Our considerations exhibit that roughness affects the static interaction potentials between the colloids and the wall, leading to a slight enrichment of the particles close to the interface which eventually results a reduction of the observed dynamics when the particles become rougher.

Keywords: Near wall dynamics, DLVO interaction, evanescent wave dynamic light scattering

1. Introduction

It is known that the dynamics of colloidal particles in solution decrease when they approach a flat and hard interface, e.g. glass surface. Further, their movement becomes directionally anisotropic due to hydrodynamic interactions between the particles and that wall. Mostly, the data analysis and interpretation of investigations related to near-wall dynamics assumed spherical particles with a perfectly smooth surface and also, when addressing the static interactions with flat surfaces. However, particles with different shape than those with spherical smooth surface have not been intensely studied.

Particles with surface roughness can be produced in a controlled manner. Such suspensions exhibit another kind of rheological characteristics compared to particle suspensions with smooth surface. Colloidal porous-shell particles in suspensions also have different characteristics such as the reduction of the flow resistance, translating into a smaller effective hydrodynamic radius. The last concept can be generally applied to flows past rough surfaces at low Reynolds numbers. Therefore, it is expected that particles with rough surface and those with porous shell, show faster near-wall dynamics as compared to equal-size particles with smooth surface.

In this work, we test this prediction experimentally by acquiring the dynamic information, using the evanescent wave dynamic light scattering technique (EWDLS), of colloidal silica particles with smooth surface and rough surface as well as of micro-porous shells. To interpret the dynamic data, we implemented a model based on standard hydrodynamic theory and accounting for DLVO particle-wall interactions to numerically calculate the particle near-wall dynamics parallel to a flat glass wall.

2. Experimental and numerical methods

For the experimental realization, particles with three different surface morphology were used: silica spheres with smooth surface (SSi), silica spheres with controlled rough surface (RSi) and spherical hollow shells (HSi). The colloidal particles were dispersed in pure water (Mili-Q, 18 MΩ*cm) with an electrolyte concentration of $c_s \approx 10^{-5}$ mol/L due to carbon-dioxide absorption which relates to a Debye length of $\lambda_D^{-1} \approx 100$ nm. Further characterization was done by means of dynamic light scattering in order to obtain their diffusion coefficient in bulk and their respective hydrodynamic radius. Such characterizations were done before and after each EWDLS experiment. In all cases, no significant variations in hydrodynamic radius were found.

In order to determine the particle near-wall dynamics parallel to the interface at a given penetration depth of the evanescent wave, the colloidal suspension was placed in the EWDLS set-up, described in Ref. [3]. A series of correlation functions were recorded in a way that the parallel component of the scattering vector was tuned in steps of θ while α_r remained fixed according with: $Q_\parallel = 2\pi n_2\sqrt{1+\cos^2\alpha_r - 2\cos\theta\cos\alpha_r}/\lambda_0$, where n_2 is the refractive index of the medium, α_r is the off-plane and θ the in-plane angles that define the detector unit's position with respect to the reflecting interface. The initial slopes of the field auto-correlation functions Γ are then determined and plotted versus $Q_\parallel^2$ to yield a linear slope. This slope represents the diffusion coefficient parallel to the interface $\langle D_\parallel\rangle(\kappa)$, integrated over the penetration depth $2/\kappa$.

The numerical model computes the near-wall dynamics of spheres, considering that particles interact with the wall by a static potential. We calculate the initial slope of the scattered field time auto-correlation function as

$$\Gamma = \frac{\int_R^\infty dz\, \exp\{-\beta\Phi(Z)\}\exp\{-\kappa z\}\langle D_\parallel\rangle(\kappa)Q_\parallel^2 + \langle D_\perp\rangle(\kappa)\left(Q_\perp^2 + \frac{\kappa^2}{4}\right)}{\int_R^\infty dz\, \exp\{-\beta\Phi(Z)\}\exp\{-\kappa z\}}$$

In this case, the particle number density is depending on the separation distance, z, different from hard sphere systems. Therefore, the averages of the diffusion constants have to be weighted by the local density written as the Boltzmann factor of the static particle wall interaction potential Φ(z), where $\beta = 1/k_BT$. The position dependent diffusion constants $D_{\parallel,\perp}(z)$ are calculated using the well-known expressions by Brenner and coworkers [1, 2] and with the definition of the averages

$$\langle D_{\parallel,\perp}\rangle(\kappa) = \frac{\int_R^\infty dz\, \exp\{-\beta\,\Phi(z)\}\exp\{-\kappa z\}\, D_{\parallel,\perp}(z)}{\int_R^\infty dz\, \exp\{-\beta\,\Phi(z)\}\exp\{-\kappa z\}}$$

the expression for Γ reduces to the linear relation

$$\Gamma = \langle D_\parallel\rangle(\kappa)Q_\parallel^2 + \langle D_\perp\rangle(\kappa)\left(Q_\perp^2 + \frac{\kappa^2}{4}\right).$$

For systems with sufficiently low polydispersity. Thus, the averaged parallel diffusion constant can be determined from the slope of a Γ vs $Q_\parallel^2$ plot. For systems with significant polydispersity or containing aggregates, the expressions for $\langle D_{\parallel,\perp}\rangle(\kappa)$ have to be additionally integrated over the particle size distribution.

The particle-wall interactions $\Phi(z)$ is modeled as the superposition of an attractive van der Waals potential (calculated for the sphere wall geometry), an electric double layer repulsion (considering the Lin et al. approach [4]) and the gravitational potential of the sphere.

3. Results

In the following figure, the experimental values of the parallel diffusion constants, normalized by their respective diffusion constant in bulk, are plotted versus the penetration depth of the evanescent wave, normalized by the particles' hydrodynamic radii in bulk. In the graph, the calculated dynamic curves are included which best match the measured data.

For the SSi and HSi systems, we could obtain a reasonable match of the calculated data with the experimental data using an amplitude of the electrostatic repulsion of the order of k_BT and some fraction of k_BT for the Hamaker constant defining the strength of the van der Waals attraction. However, in the case of the RSi system, the Hamaker constant required to make the calculated data match with experimental data is an order of magnitude larger than for the SSi and HSi systems. This implies that surface roughness plays an important role for the particle wall interaction and thus, the resulting near wall dynamics. On the other hand, we found that the effect of sedimentation on the particle dynamics is negligible as compared to the DLVO interactions, for the particle sizes used here.

Our findings are in line with earlier simulation works [5, 6] which showed that surface roughness enhances the strength of both, electrostatic repulsion and van der Waals attraction. However due to the different distance dependence of the two interaction types, a reduction of the stabilization barrier of the resulting DLVO interaction potential occurs and the primary minimum becomes shallower or disappears completely for certain degrees of roughness. These effects are attributed to the effective surface to surface separation which is reduced by the asperities on the surface. With this in mind, our results are the first experimental evidence of the roughness effects on DLVO interaction potentials predicted by simulations. **14**, 3365-3375, 1998.

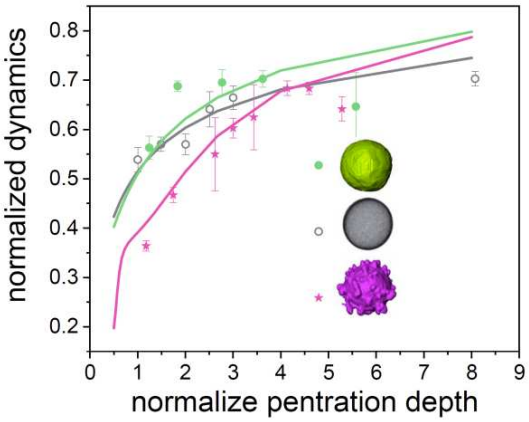

Figure 1: Normalized parallel near-wall diffusion coefficients of the three types of particles. Symbols are experimental data with their corresponding standard deviation (error bars). Solid lines represent the numerical predictions. The colours correspond to particle type: green to smooth particles; grey to hollow shells; and pink to rough particles. *Image from ref. [3]*.

4. Conclusions

We have found that suspension of particles with smooth surface and the suspension of hollow porous shells, have qualitatively similar parallel near-wall dynamics as hard-sphere systems (not shown here). However, suspensions of rough surface particles exhibit slower parallel near-wall dynamics than the systems mentioned above. In order to understand these behaviours of the systems, we performed numerical calculation of the dynamics considering static particle-wall interactions. The most striking result was observed for the rough particle suspension where the Hamaker constant, needed to reach the experimental data, was at least five times larger than the Hamaker constant for the other two systems.

This work contributes to considerations on the near-wall dynamics of colloidal suspensions; when the surface morphology of the particles is rough, static particle-wall interactions can overcompensate hydrodynamic effects.

References

[1] Goldman A. J., Cox R. G. and Brenner H., *Chem. Engineering Science*, **22**,637-651, 1967
[2] Brenner H., *Chem. Engineering Science*, **16**, 242–251 1961.
[3] Rivera-Morán, J. A., Liu, Y., Monter, S., Hsu, C.-P., Ruckdeschel, P., Retsch, M., Lisicki, M. and Lang, P. R., *Soft Matter,* DOI: 10.1039/D1SM01191J 48
[4] Lin, S. and Wiesner, M. R., *Langmuir,* **26**, 16638-16641, 2010.
[5] Walz, J. Y., *Particles on Surfaces*, **7**, 151-169, 2002.
[6] Bhattacharjee, S., Ko, C.-H. and Elimelech, M., *Langmuir*, **14**, 3365-3375, 1998.

Rotating spherical particle in a continuous viscoelastic medium — a microrheological example situation

S. K. Richter, C. D. Deters, and A. M. Menzel
Institut für Physik, Otto-von-Guericke-Universität Magdeburg
Universitätsplatz 2, 39106 Magdeburg, Germany
sonja.richter@ovgu.de

Abstract

Theoretical studies can provide means by which to extract from microrheological investigations the properties of viscoelastic materials. Concentrating on the response of an embedded particle in a one-component viscoelastic medium, we intend to determine material properties from the response that the particle shows to an external torque. For the description of the medium, which can feature fluid-like behavior with a net flow, elastic behavior with damped reversible dynamics, or anything between these two limits, we introduce a relaxation parameter. It allows us to interpolate between the limiting cases. Specifically, we consider a rigid, magnetically anisotropic, spherical inclusion, which rotates in response to an external torque exerted by a magnetic field. Additionally, we quantify the induced deformation and flow fields in the surrounding medium.

Keywords: Active microrheology, linear viscoelasticity, susceptibility, probe particle

1. Introduction

In active microrheology, the response of embedded probe particles to externally applied stimuli is used to extract properties of the surrounding medium [1]. We describe the coupling between a spherical probe particle and its one-component viscoelastic environment while an external torque is applied together with distortions and flows induced in the viscoelastic medium. For example, the torque can be generated by an external magnetic field applied to a magnetically anisotropic particle. Figure 1 illustrates the situation of one particle that rotates around the axis along which the torque is applied.

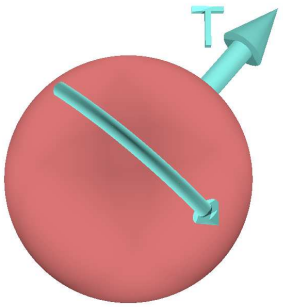

Figure 1: Embedded particle in a one-component viscoelastic medium exposed to a torque $\mathbf{T}$ that induces rotations.

2. Viscoelastic medium

We investigate a one-component viscoelastic material that features a fluid-like part as well as an elastic part of its mechanical response. The dynamic transport is described by a flow field $\mathbf{v}(\mathbf{r},t)$ and the elastic memory by a displacement field $\mathbf{u}(\mathbf{r},t)$. In combination, at low Reynolds number, and after linearization, corresponding continuum equations [2] turn into

$$\mu\nabla^2\mathbf{u}(\mathbf{r},t)+\eta\nabla^2\mathbf{v}(\mathbf{r},t)=\boldsymbol{\nabla}p(\mathbf{r},t)-\mathbf{f}_b(\mathbf{r},t) \tag{1}$$

[3], with the elastic shear modulus μ, dynamic viscosity η, pressure field $p(\mathbf{r},t)$, and bulk force density $\mathbf{f}_b(\mathbf{r},t)$. The transport and relaxational behavior contributing to the dynamics of the memory field $\mathbf{u}(\mathbf{r},t)$ are quantified via

$$\dot{\mathbf{u}}(\mathbf{r},t)=\mathbf{v}(\mathbf{r},t)-\gamma\mathbf{u}(\mathbf{r},t) \tag{2}$$

with the relaxation parameter γ of the elastic memory. This parameter allows us to distinguish between perfectly elastic media ($\gamma=0$), the viscous hydrodynamic limit ($\gamma\to\infty$), and all intermediate viscoelastic situations bounded by these limits. To describe the rotation of a particle that is embedded in the viscoelastic medium, an analogous relation of the particle rotation and the angular velocity is implied.

3. Particle reorientations through magnetic fields

Our particle is assumed to be uniformly magnetized, homogeneous, magnetically hard, and to carry a permanent magnetic dipole moment $\mathbf{m}(t)$ of constant magnitude m anchored to the particle frame. The environment is nonmagnetic. We calculate the linear rotational response in terms of the reorientation angle $\delta\varphi$ of the particle in reaction to a torque exerted by a homogeneous external magnetic field that oscillates with frequency ω.

4. Linear response function and magnetic susceptibility

Next, we define a linear response function for the angular reorientation

$$\chi_\varphi(\omega)=\chi'_\varphi(\omega)-\mathrm{i}\chi''_\varphi(\omega) \tag{3}$$

and put it in context to the before-determined angular response $\delta\varphi$. In experiments with many particles the induced overall magnetization is a measurable quantity. Then χ is the dynamic magnetic susceptibility, where χ' corresponds to its storage and χ'' to

its loss part. Our calculated susceptibility reads

$$\tilde{\chi}'(\tilde{\omega}) = \frac{1}{\tilde{\omega}^2 + (1+\mathcal{V})^2} \tag{4}$$

$$\tilde{\chi}''(\tilde{\omega}) = \frac{1}{\tilde{\omega}} \left(1 - \frac{1+\mathcal{V}}{\tilde{\omega}^2 + (1+\mathcal{V})^2}\right) \tag{5}$$

with $\mathcal{V} = \gamma\eta/\mu$, and the tilde indicates suitable rescaling.

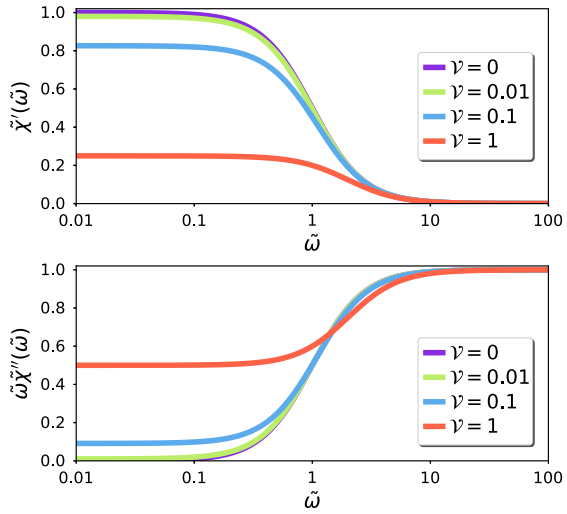

Figure 2: Rescaled storage and loss parts χ' and χ'' of the magnetic susceptibility as a function of the rescaled frequency $\tilde{\omega}$. Partly reproduced from Ref. [4]. ©IOP Publishing. Reproduced with permission. All rights reserved (DOI:10.1209/0295-5075/134/68002).

In Fig. 2 this susceptibility is plotted for different values of $\mathcal{V}$. For a perfectly viscous surrounding ($\mathcal{V} \to \infty$) we see that $\tilde{\chi}'(\tilde{\omega}) \to 0$ and $\tilde{\omega}\tilde{\chi}''(\tilde{\omega}) \to 1$, which means $\tilde{\chi}''(\tilde{\omega}) \to 1/\tilde{\omega}$. Thus the medium does not store any elastic energy. Conversely, for a perfectly elastic medium ($\mathcal{V} = 0$) and quasistatic dynamics ($\tilde{\omega} \to 0$), we find $\tilde{\chi}'(\tilde{\omega}) \to 1$ and $\tilde{\chi}''(\tilde{\omega}) \to 0$, which indicates complete permanent storage of deformation energy. The viscoelastic situations $0 < \mathcal{V} < \infty$ lead to intermediate results. We note that χ'' diverges for any $\mathcal{V} > 0$ as $\tilde{\omega} \to 0$, but tends to zero for the perfectly elastic case of $\mathcal{V} = 0$.

5. Explicit fields

The time-dependent memory displacement field in a viscoelastic environment for $r \geq a$ follows from

$$\mathbf{u}(\mathbf{r}, t) = -\frac{1}{2}\int_{-\infty}^{\infty} \mathrm{d}t'\, G(t-t')\mathbf{T}(t') \cdot [\boldsymbol{\nabla} \times \underline{\mathbf{G}}(\mathbf{r})], \tag{6}$$

where a is the particle radius, $\mathbf{T}(t)$ is the time-dependent torque, and $\underline{\mathbf{G}}(\mathbf{r})G(t)$ is the Green's function that solves Eqn (1). In a second step, via Eqn (2), the flow field $\mathbf{v}(\mathbf{r}, t)$ can be directly calculated. So additionally to the resulting particle rotation, we can determine the induced flows and distortions in the surrounding viscoelastic medium. In the limiting case of a perfectly elastic medium the displacement field is in phase with the driving field, while for a viscous fluid the flow field is in phase.

6. Perspective

By fitting the above expressions to measurement results, material properties of a one-component viscoelastic material can be determined. Specifically, this applies to the elastic shear modulus μ, the dynamic viscosity η, and the parameter γ associated with the elastic memory. We hope to support by our analysis and derivation corresponding microrheological investigations of one-component viscoelastic materials in the future.

References

[1] MacKintosh, F. C., and Schmidt, C. F., Microrheology, *Curr. Opin. Colloid Interface Sci.*, 4, pp. 300-307, 1999.

[2] Temmen, H., Pleiner, H., Liu, M., and Brand, H. R., Convective nonlinearity in non-Newtonian fluids, *Phys. Rev. Lett.*, 84, pp. 3228–3231, 2000.

[3] Puljiz, M., and Menzel, A. M., Memory-based mediated interactions between rigid particulate inclusions in viscoelastic environments, *Phys. Rev. E*, 99, 012601, 2019.

[4] Richter, S. K., Deters, C. D., and Menzel, A. M., Rotating spherical particle in a continuous viscoelastic medium — a microrheological example situation, *EPL (Europhys. Lett.)*, 134, 68002, 2021.

Topology controls the emergent dynamics in nonlinear flow networks: towards a excitable fluidic system

Miguel Ruiz-Garcia[1,2], Alejandro Martinez-Calvo[3,4] and Eleni Katifori[2]

[1]*Department of Mathematics, Universidad Carlos III de Madrid, 28911 Leganés, Spain*

[2]*Department of Physics and Astronomy, University of Pennsylvania, Philadelphia, Pennsylvania 19104, USA*

[3]*Department of Chemical and Biological Engineering, Princeton University, Princeton, NJ 08544, USA*

[4]*Princeton Center for Theoretical Science, Princeton University, Princeton, NJ 08544, USA*

Abstract

Flow networks are essential for both living organisms and engineered systems. These networks often present complex dynamics controlled, at least in part, by their topology. Previous works have shown that topologically complex networks interconnecting explicitly oscillatory or excitable elements can display rich emerging dynamics. Here we present a model for complex flow networks with non-linear conductance that allows for internal accumulation/depletion of volume, without any inherent oscillatory or excitable behavior at the nodes. In the absence of any time dependence in the input and output we observe emerging stationary pattern formation and complex dynamics in the form of self-sustained waves, which travel through the system. The frequency of these waves depends strongly on the network architecture and it can be explained with a topological metric. Our results can be tested in networks of quantum wells or using fluidic flow networks that present negative differential conductivity elements. We briefly describe how to build such systems in the fluidic realm.

Keywords: flow networks, negative differential conductivity, topology, fluid-structure interactions

Flow networks are necessary when nature or humans need to distribute resources, such as water, nutrients or power. On the other hand, artificial microfluidic networks are rapidly evolving, incorporating more elaborated topologies and non-linear elements. Inspired by the spontaneous oscillations in mammalian cortex hemodynamics –at least part of these fluctuations seem to correspond to non-neuronal processes– we have proposed a model for non-linear flow networks that exhibit spontaneous oscillations [1]. Whereas [1] focused on the conditions that lead to the appearance of spontaneous fluctuations in one-dimensional networks, here we explore to what extent oscillations or fluctuations in flow networks of an arbitrary topology can emerge spontaneously, in the absence of a time-modulating external stimulus, as a product of internal non-linearities. Additionally, we show how the frequency and amplitude of the oscillations depends on the network structure, and that this dependence can be explained using a simple network metric. The details of the model can be found in [1, 2], we define a network as a set of N nodes and connections between them (edges). Pressures (P_i) and accumulated volumes (V_i) are defined at each node i and the volumetric current I_{ij} is defined on edge ij. The current I_{ij} depends on the pressure difference $\Delta P_{ij} = P_i - P_j$ following a general pressure flow relation:

$$I_{ij} = \begin{cases} \frac{1}{2} V_i^2 \Gamma(\Delta P_{ij}), & \text{if } P_i > P_j \\ \frac{1}{2} V_j^2 \Gamma(\Delta P_{ij}), & \text{if } P_j > P_i \end{cases} \tag{1}$$

In this work, Γ can display two different behaviors, either linear or nonlinear:

$$\Gamma_L(\Delta P) = h\Delta P, \quad \Gamma_{NL}(\Delta P) = \frac{\Delta P_0^4 + \epsilon \Delta P^4}{\Delta P_0^4 + \Delta P^4} \Delta P, \tag{2}$$

where ϵ and h are dimensionless parameters that determine the shape of the non-linearity in Γ_{NL} and the slope of Γ_L, and P_0 is a constant value. We choose a Γ_{NL} such that it has a negative slope region. See [1] for different biological and engineered systems where this non-monotonic relation is present. Conservation of volume imposes the temporal variation of the accumulated volume at every node,

$$\dot{V}_i = \sum_j -I_{ij}. \tag{3}$$

Finally, we include a constitutive relation that couples the excess volume from a baseline (set to V_0), to the curvature of the pressure:

$$V_i - V_0 = \alpha \sum_j L_{ij} P_j. \tag{4}$$

α is a constant, L_{ij} is the ij element of the graph Laplacian $L = D - A$, where D is the degree matrix and A is the adjacency matrix. This pressure-volume relationship is a phenomenological expression consistent with the physics of flow through an elastic medium [1]. From equations (3) and (4) we get:

$$\alpha \sum_j L_{ij} \dot{P}_j = -\sum_j I_{ij}, \tag{5}$$

which is the system of ordinary nonlinear differential equations that, together with the boundary conditions (externally set pressures) is propagated in time to produce the results presented in this work.

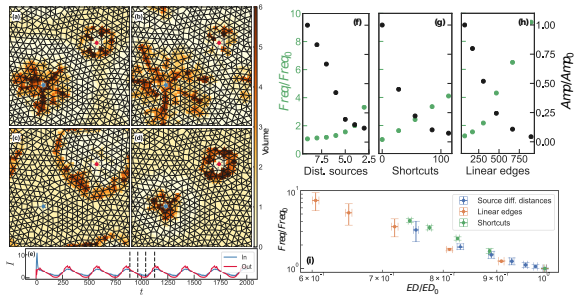

Figure 1: Self-sustained waves in a disordered planar network with periodic boundary conditions. In (a)-(d), continuous and gray dashed lines correspond to Γ_{NL} and Γ_L, respectively. We color the area around each node according to V_i. A constant pressure is imposed at the contact points (blue and red dots). (e) Total current going in and out of the system versus time, vertical dashed lines mark the time at which each snapshot (a)-(d) was taken. We study the frequency and amplitude of the spontaneous oscillations when: f) The two contacts are randomly placed at a specified distance. (g) Contacts are at a fixed distance whereas the topology of the network is changed adding shortcuts. (h) We replace a set of edges chosen at random with linear edges. (i) All frequency points collapse on a single curve when plotted against the normalized effective distance (ED), inversely proportional to the escape probability of a random walk.

When we impose a constant pressure difference between two nodes, the accumulated volume displays self-sustained oscillations in the form of pulses that travel from the high to the low pressure contact point (see Fig. 1 (a)-(d)). In Fig. 1 (f)-(h) we study how the nature of the spontaneously emerging oscillations changes as the distance between the contact points (sources) decrease, as the network becomes more interconnected, or as we increase the fraction of linear edges. As the pulses travel from one contact to the other, the time that they take to travel through the system will decrease as the distance between the contacts is reduced, making the frequency go up. We therefore propose an *effective network distance* that unifies all the structural modifications. This is a purely topological metric that characterizes the structure of the network. We resort to the escape probability of a random walk (RW). The escape probability increases as the two contacts are moved closer to each other. Likewise, adding random shortcuts create new shorter paths between the two contacts, this way also increasing the escape probability. Finally, linear resistors result in the pulse traveling much faster through them. Therefore, when the RW lands on a node connected to one or more linear edges it will not traverse the non-linear ones in the next step. Instead, it will use, with equal probability, one of the linear edges [2]. Fig. 1 (i) shows all the frequency data points presented in the top three panels. On the horizontal axis we use the inverse of the escape probability for every configuration – which we term effective distance. This allows us to plot all the points resulting from the three different modifications of the network as a function of the same topological metric. All points on Fig. 1 (i) lay on the same curve, suggesting that the effective distance is a meaningful measure to characterize an important part of the emerging dynamics in this system.

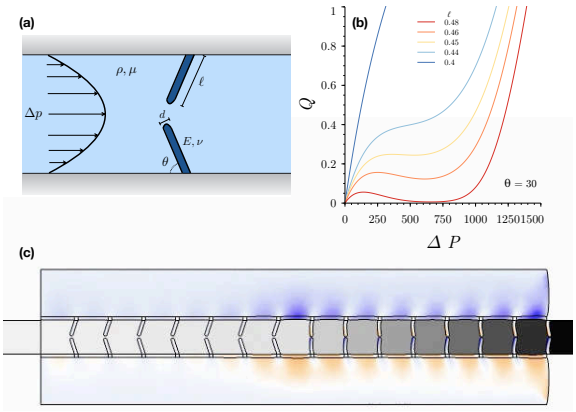

Figure 2: Prototype of a 1D fluidic network with negative differential conductivity. Panel (a) shows a valve that can display negative differential conductivity depending on the angle and length of the beams. Panel (b) displays the flow versus pressure difference relation for this valve. We chose a 30 degrees angle and different lengths. Panel (c) shows the stationary behavior of a system with 15 valves.

At the end of this talk we will present our current work directed to build this kind of flow network in the lab. Figure 2 presents a small prototype simulated using *COMSOL*. Figure 2 (a) shows a valve that can display negative differential conductivity. Depending on the angle and length of the beams, their flow versus pressure difference relation displays a region of negative slope, analogous to Γ_{NL} in Eq. (2), see Fig. 2 (b). Finally, panel 2 (c) shows a snapshot of a system with 15 valves. This prototype already displays complex dynamics. In this case the system finds a stationary state where half the valves are open (low pressure drop region) and the other half are highly deformed (high pressure drop region), this is in good agreement with our theory, see [1] for more details.

In summary, this work shows that a network of nonlinear *passive* resistors of arbitrary topology can support emerging dynamics even in the absence of a time varying input. Furthermore, the relation between the frequency of the oscillations and the structure of the network can be explained through a simple network metric. Previous models for excitability in complex networks used expressions for already excitable elements that were connected within a complex network. These elements broadly belonged to two different classes: they were discrete variables that could be in a resting, excited or refractory state and that could excite their neighbors; or they could be neuron-like continuous variables whose dynamics were coupled to their neighbors' dynamics. In our work the nodes are not intrinsically excitable neither oscillatory, but simply store volume. Excitability emerges as a global effect that stems from the combination of: (i) the coupling between the stored volume and the pressure field and (ii) the nonlinear conductance of the edges. This combination gives rise to the complex dynamics shown, at least in part, in this work.

References

[1] Ruiz-García, M., and Katifori, E., Emergent dynamics in excitable flow systems, *Physical Review E* 103.6, 062301, 2021.

[2] Ruiz-Garcia, M., and Katifori, E., Topologically controlled emergent dynamics in flow networks, *arXiv preprint*, arXiv:2001.01811, 2020

Two-dimensional diffusion biased by a transverse gravitational force in an asymmetric channel

Ivan Pompa-García[1✉] **and Leonardo Dagdug**[1,2§]

[1] *Universidad Autónoma Metropolitana - Iztapalapa*
Av. San Rafael Atlixco 186, Leyes de Reforma 1ra Sección, Iztapalapa, 09340, Ciudad de México, México
✉ *Presenting author: ivanjpg@xanum.uam.mx*

[2] *National Institutes of Health, Shriver National Institute of Child Health and Human Development*
29 Lincoln Drive, Building 29B, Bethesda, MD 20892, U.S.
§ *Corresponding author: dll@xanum.uam.mx*

Abstract

Using the projection method by Kalinay and Percus [J. Chem. Phys. 122, 204701 (2005)], we derive an effective diffusion coefficient for narrow channels that generalizes previously reported results. This is, a position-dependant diffusion coefficient for two-dimensional asymmetric channels under a transverse gravitational external field is obtained. The main result, shown in equation (5), contains the well-known previous results for symmetric channels with external gravitational force presented by Kalinay [Phys. Rev. E 84, 011118 (2011)], as well as asymmetrical cases where the transverse field goes to zero. Also, found coefficient can be approximately written as an interpolation formula as proposed initially by Reguera and Rubi [Phys. Rev. E 64, 061106 (2001)], can be used to recover preceding results as well. Finally, the excellent agreement of equations (5), (6) and (7) with Brownian dynamics simulations is shown.

Keywords: ICSTCF2021, brownian motion, random walks, confined diffusion

1. Introduction

The diffusion coefficient is a quantity that can be used to describe transport in a system. For a free system, it is customary to use a diffusion constant (D_0). Once confinement or external field influence is imposed, it is needed to extend the model by using the effective diffusive coefficient (D_{eff} or $D(x)$) that, in this case, depends on the x-coordinate. Second Fick's law provides us [1] with a basic description of free systems but Fick-Jacobs [2] and even better, Fick-Jacobs-Zwanzig [3] equations improve the models. Later Reguera and Rubi proposed [4] a new heuristically-found coefficient enhancing Zwanzig's result. Kalinay and Percus used their method [5], named projection method [6] to make an even better description of diffusive systems. The last procedure was used by Kalinay himself [7] to describe a symmetrical channel under transverse gravitational force.

2. Projection Method

A brief outline of the projection method can be stated as follows. We write the bidimentional Smoluchowski equation [8]

$$\frac{\partial \rho(x,y,t)}{\partial t} = \left(D_x \frac{\partial}{\partial x} e^{-\beta U(x,y)} \frac{\partial}{\partial x} e^{\beta U(x,y)} + D_y \frac{\partial}{\partial y} e^{-\beta U(x,y)} \frac{\partial}{\partial y} e^{\beta U(x,y)} \right) \rho(x,y,t), \tag{1}$$

choosing for this particular case a gravitational-like potential $U(y) = Gy$, where $g \equiv \beta G$. Now the one-dimentional density is calculated by taking the integral of the particle density $\rho(x,y,t)$

$$c(x,t) = \int_{h_1(x)}^{h_2(x)} \rho(x,y,t)\, dy. \tag{2}$$

This should be done inside the system's boundaries. The next step is to obtain an equilibrium solution for density by assuming $D_y \to \infty$, this is a transverse-directional equilibrium. This solution can be easily written as

$$\rho_0(x,y,t) = \frac{1}{A(x)}\, e^{-gy} c(x,t), \tag{3}$$

where $A(x)$ is a normalization function that contains boundaries and potential information encoded inside. Now we can see ρ as the result of a perturbative series in $\epsilon \equiv D_x/D_y$

$$\rho(x,y,t) = e^{-gy} \sum_{n=0}^{\infty} \epsilon^n \hat{\omega}_n(x,y,\partial_x) \frac{c(x,t)}{A(x)}, \tag{4}$$

applying the usual techniques for series solutions and the key assumption of a stationary regime for long times ($\partial_t c(x,t)$) we can found $D(x)$.

3. Results

The known results for two-dimensional narrow channels could be generalized by

$$\begin{aligned} \frac{D(x)}{D_0} = 1 &- \frac{w'^2(x)}{4\sinh^2\left[\frac{1}{2}gw(x)\right]} \\ &\times \left\{ 1 + \cosh^2\left[\frac{1}{2}gw(x)\right] - gw(x)\coth\left[\frac{1}{2}gw(x)\right] \right\} \\ &- y_0'(x) \left\{ y_0'(x) - w'(x)\coth\left[\frac{1}{2}gw(x)\right] \right. \\ &\left. + \frac{1}{2}gw(x)w'(x)\,\mathrm{csch}^2\left[\frac{1}{2}gw(x)\right] \right\}, \end{aligned} \tag{5}$$

and approximately written using an interpolation formula

$$D_\eta(x) = \frac{D_0}{\left[1+\frac{1}{4}w'^2(x)\right]^\eta}, \tag{6}$$

where

$$\eta = \frac{1}{\sinh^2\left[\frac{1}{2}gw\right]}\left\{1+\cosh^2\left[\frac{1}{2}gw\right] - gw\coth\left[\frac{1}{2}gw\right]\right\} + 4\frac{y_0'}{w'^2}\left\{y_0' - w'\coth\left[\frac{1}{2}gw\right] + \frac{1}{2}gww'\,\mathrm{csch}^2\left[\frac{1}{2}gw\right]\right\}. \tag{7}$$

Above equations contains the channel width $w(x) = h_2(x) - h_1(x)$, the midline $y_0(x) = [h1(x) + h_2(x)]/2$ and their respective derivatives.

4. Brownian Dynamics Simulations

Simulations where performed using Fortran & C codes, paralellizing the exection of the programs. All realizations were made with $\Delta t = 10^{-6}$, 10^7 steps and 2.5×10^4 particles. The probe channels has a period of $L = 1$. First simulation round was conducted with channel boundaries' defined by $h_2(x) = [\sin(2\pi x) + 1.02]/(2\pi) = -h_1(x)$ and a G magnitude transversal force. Following simulations were completed changing the lower boundary to be $h_1(x) = 0$ and transversal constant force in two different directions $+G$ and $-G$.

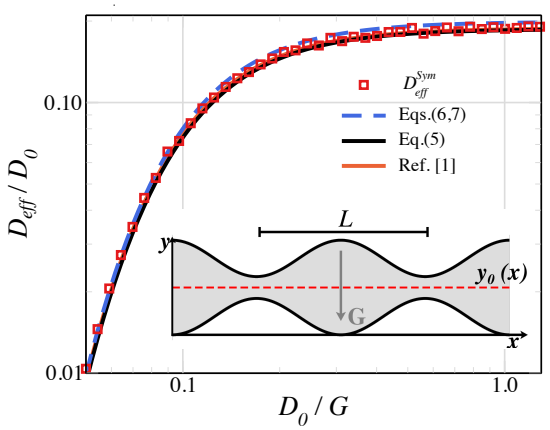

Figure 1: Effective diffusion coefficients obtained numerically in Ref. [9] (continuous red line), those predicted by equation (5) (continuous black line), and the interpolation formula given by equations (6) and (7) (dashed blue line), are compared with the values obtained by Brownian dynamics simulations (square red symbols). The boundaries of the channel are defined by the dimensionless function $h_2(x) = -h_1(x) = [\sin(2\pi x)+1.02]/2\pi$, subjected to a constant perpendicular G force. L gives the periodicity of the channel [9]. In the inset the straight midline is shown as a red dotted line.

5. Conclusions

The newly obtained Eq. (5) allows us to recover the Kalinay results [7] by considering a symmetric channel with zero midline. Reguera and Rubi expression [4] arises when the transversal force is null. Also, Bradley model [10] can be gathered if the asymmetry of the system is maintained but the transverse external field is removed. Some interesting behavior is predicted for the diffusion coefficient by setting $G \to -\infty, +\infty$, where $D_0/\left[1+h_2'^2(x)\right]$ and $D_0/\left[1+h_1'^2(x)\right]$ respectively, this can be promising in order to achieve particle separation and diffusion coefficient control at will by turning on and off the external field or tuning its magnitude.

Also, it is remarkable how Eq. (5) can be recovered by taking the first two terms of the series obtained from Eqs. (6) and (7) as Reguera and Rubi [4], and Kalinay [7] proposed. Furthermore, the asymmetry and boundaries information of the system can be encoded into the η exponent.

The Brownian dynamics simulations and Eqns. (5), (6), and (7) are in excellent agreement. Additionally, the symmetrical case was compared to the predicted behavior found by another methods as shown in Ref. [9].

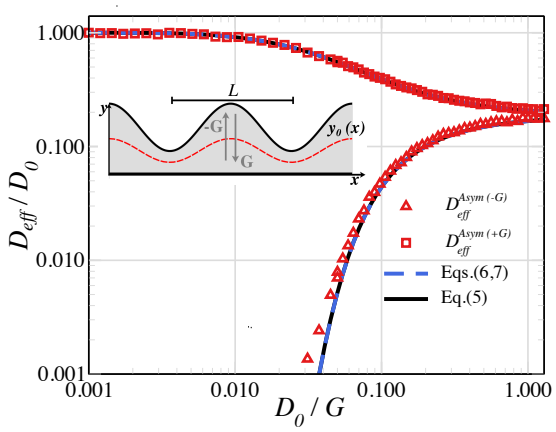

Figure 2: Effective diffusion coefficients predicted by equation (5) (continuous black line), and the interpolation formula given by equations (6) and (7) (dashed blue line), are compared with the values obtained by Brownian dynamics simulations (red square and triangle symbols). The boundaries of the channel are defined by the dimensionless function $h_2(x) = [\sin(2\pi x) + 1.02]/2\pi$ and $h_1(x) = 0$, subjected to a constant perpendicular G force. L gives the periodicity of the channel [9]. In the inset the curved midline is shown as a red dotted line.

References

[1] D. A. Fick, London, Edinburgh Dublin Philos. Mag. J. Sci., 30 (1855).

[2] M. H. Jacobs, in *Diffusion Processes* (Springer Berlin Heidelberg, Berlin, Heidelberg, 1935), p. 145.

[3] R. Zwanzig, J. Chem. Phys. **96**, 3926 (1992).

[4] D. Reguera and J. M. Rubí, Phys. Rev. E **64**, 061106 (2001).

[5] P. Kalinay and J. K. Percus, J. Chem. Phys. **122**, 204701 (2005).

[6] P. Kalinay and J. K. Percus, Phys. Rev. E **74**, 041203 (2006).

[7] P. Kalinay, Phys. Rev. E **84**, 011118 (2011).

[8] M. von Smoluchowski, Annalen der Physik **326**, 756 (1906).

[9] P. S. Burada and G. Schmid, Phys. Rev. E **82**, 051128 (2010).

[10] R. M. Bradley, Phys. Rev. E **80**, 061142 (2009).

Vortices in an active matter system based on magnetic beads under an alternating magnetic field

A. Escobar[1] **and F. Donado**[2]

[1] *Instituto de Ciencias Básicas e Ingeniería de la Universidad Autónoma del Estado de Hidalgo-AACTM,*

Km. 4.5 Carr. Pachuca-Tulancingo, Carboneras, Mineral de la Reforma, Hidalgo, México
e-mail: angeles_escobar19@hotmail.com

[2] *A Instituto de Ciencias Básicas e Ingeniería de la Universidad Autónoma del Estado de Hidalgo-AAMF,*

Km. 4.5 Carr. Pachuca-Tulancingo, Carboneras, Mineral de la Reforma, Hidalgo, México
e-mail: fernando@uaeh.edu.mx

Abstract

We study the origin and characteristics of vortices in an active matter system composed of magnetic particles that independently take energy from an alternating magnetic field and convert it into kinetic energy. The system works under stationary conditions even though it is highly dissipative, thanks to the continuous energy input from the field. At high particle concentration, we observed the formation of vortices. We study their behavior and characteristics under different particle concentrations. The system lets us study individual particle motion. We discuss how vortices arise based on the dynamics of particles obtained from the mean squared displacement. We used order parameters to describe the structural characteristics of the system.

Keywords: active matter, vortices, nonvibrating granular system

Active and passive brownian particles in external fields

A. L. Merino-Díaz, R. Ramírez-Sánchez and E. Ramírez-solano
Facultad de Ciencias Físico Matemáticas, Benemérita Universidad Autónoma de Puebla
Avenida San Claudio y 18 Sur, Colonia San Manuel, Edificio FM1-101B, Ciudad Universitaria, C.P. 72570, Puebla, México
laura.diaz.fisica@gmail.com

Abstract

Active particles, unlike passive ones, can convert energy from their environment into directed motion. In recent years, these particles have been studied with applications in medicine and transportation. In this work, we use Langevin equation formalism to describe the movement of an infinitely diluted colloid of active Janus particles in an external constant electric field. The spherical active Janus particle, with swim velocity of constant magnitude has a dipolar momentum that interacts with the field. We want to analize the traslational and orientational mean square displacement (MSD) when the intensity of the field change as well as the velocity of the particle with a Weeks-Chandler-Andersen potential (WCA). The MSD reveals that the system stabilizes rapidly when the intensity of the magnetic field is higher and the propulsion speed lower.

Keywords: Active matter, Janus particle, magnetic field

1. Introduction

A Janus active particle is a kind of particle whose surface chemically interacts with the solvent to generate mechanical movement. We focus on a Janus particle with a dipole on it's center of mass [1].

Through Brownian Dynamics we want to calculate the Mean Square Displacement (MSD) to study the behavior of the particle when two factors change: the magnetic external field that interacts with the dipole and the velocity of the particle when interacts with the WCA potential.

2. Metodology

For the Brownian dynamics we use the Langevin formalism [2]. The equations that describe the active system includes a therm of propulsion velocity ($v_0\hat{\mathbf{u}}$), that particles use to move regardless thermal bath, also includes the therms of the force and torque due to the external field $\mathbf{E}$ that interacts with the dipole of the Janus particle $\boldsymbol{\mu} = \mu\hat{\mathbf{u}}$, [3, 4]. So, the position $\mathbf{r}$ and orientation $\hat{\mathbf{u}}$ at time $t + \delta t$ are given by

$$\mathbf{r}(t+\delta t) = \mathbf{r}(t) + \delta t\, v_0\, \hat{\mathbf{u}}(t) + \frac{\delta t}{\gamma_t}\boldsymbol{\xi}_t(t) + \frac{\delta t}{\gamma_t}\mathbf{f}(t), \quad (1)$$

$$\hat{\mathbf{u}}(t+\delta t) = \hat{\mathbf{u}}(t) + \frac{\delta t}{\gamma_r}\boldsymbol{\xi}_r(t) + \frac{\delta t}{\gamma_r}\left(\boldsymbol{\tau}\times\hat{\mathbf{u}}\right). \quad (2)$$

Where $\boldsymbol{\xi}_t(t)$ and $\boldsymbol{\xi}_r(t)$ are the random displacements due to the thermal bath which mean is zero and correlation is a delta function [5].

We use the cartesian coordinate system to found the position $\mathbf{r} = (x, y, z)$ and, for the orientational movement, we use spheric coordinates due to the unit vector moves in a unit sphere.

Now, the system is under a WCA potential so the force is given by $\mathbf{f}^{WCA}(\mathbf{r}_{ij}, t) = -\nabla\Phi_{WCA}$ [6], and the magnetic potential gives the form for the magnetic force $\mathbf{f}^{ext}(\mathbf{r}, t) = -\nabla\Phi_{ext}$ where $\boldsymbol{\phi}_{ext}(\mathbf{r}, \hat{\mathbf{u}}) = \boldsymbol{\mu}\cdot\mathbf{E} = \mu E(\hat{\mathbf{u}}\cdot\hat{\mathbf{z}})$. So, this two forces are

$$\mathbf{f}^{WCA}(\mathbf{r}_{ij}, t) = -24\epsilon\left[2\left(\frac{\sigma}{r_{ij}}\right)^{12} - \left(\frac{\sigma}{r_{ij}}\right)^{6}\right]\frac{\mathbf{r}_{ij}}{r_{ij}^2}, \quad (3)$$

$$\mathbf{f}^{ext}(\mathbf{r}, t) = \mu E\left[\left(\frac{xz}{r^3}\right)\hat{\imath} + \left(\frac{yz}{r^3}\right)\hat{\jmath} - \left(\frac{1}{r} - \frac{z^2}{r^3}\right)\hat{k}\right], \quad (4)$$

where $\mathbf{r}_{ij}$ is the vector between the particles i and j, $r = |\mathbf{r}|$ for all particles. The dimensionless form of the interaction force between particles are obtained considering $r' = r/\sigma$, $F' = F(\sigma/\epsilon)$.

For the internal and external torque we need to use the dipole-dipole potential and the external field so: $\boldsymbol{\mathcal{T}}^{int} = \hat{\mathbf{u}}\times\nabla_{\hat{\mathbf{u}}}\Phi_D$ and $\boldsymbol{\mathcal{T}}^{ext} = \hat{\mathbf{u}}\times\mathbf{E}$ with $\boldsymbol{\mu} = (\mu_x, \mu_y, \mu_z)$ and the field $\mathbf{E} = (0, 0, E)$, such that

$$\boldsymbol{\mathcal{T}}^{int}(\mathbf{r}_{ij}, \hat{\mathbf{u}}_i, \hat{\mathbf{u}}_j, t) = \frac{\mu^2}{r_{ij}^3}\left[3(u_j\cdot\mathbf{r}_{ij})\hat{\mathbf{u}}_i\times\mathbf{r}_{ij} - \hat{\mathbf{u}}_i\times\hat{\mathbf{u}}_j\right], \quad (5)$$

$$\boldsymbol{\mathcal{T}}^{ext}(\mathbf{r}_{ij}, t) = (E\mu_y)\hat{\imath} - (E\mu_x)\hat{\jmath}. \quad (6)$$

for this work we only use equation (6) for orientation. The equations for orientation and traslation are correlated in time, so it is necesary to calculate the orientation before the position vector.

3. Results

The change of the intensity of the external field when we have a constant velocity can be seen in the change of the positions *x,y,z* (see Figure 1).

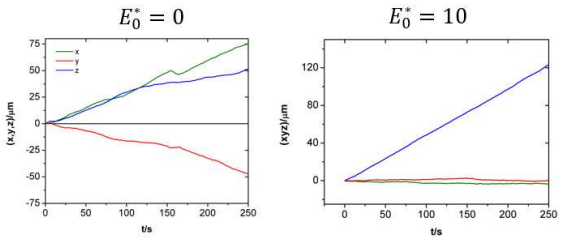

Figure 1: The change in the intensity of the field guides the particle in the same direction, this provoques that the coordinate z increasse more than the others coordinates.

To observe the behavior of the particle we graph the MSD vs Δt when the intensity of the external field changes as the velocity do. The Figures 2 show a slow displacement of the parricle when the velocity of the particle is low.

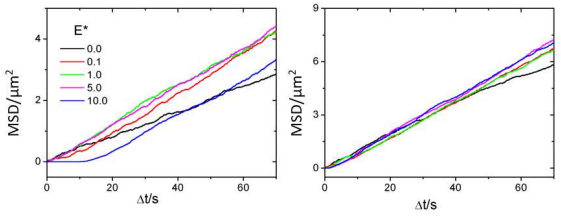

Figure 2: MSD according to time Δt, for $v_0 = 2.2\mu m/s$ (left) and $v_0 = 3.1\mu m/s$ (right). The field intensity changes according to the lines.

The behavior of the interaccion of 8 particles (diluete system) can be seen with the MSD orientational and traslational. In the next figures, when the system is absent of the external field, and with mayor velocity of the particle, the MSD increasse.

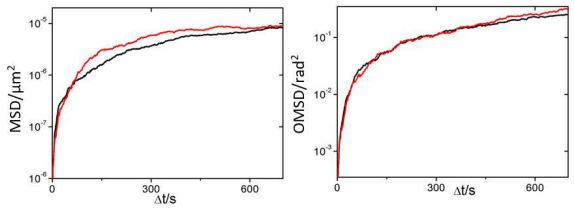

Figure 3: Traslational (left) and orientational (right) MSD for several particles when $E = 0$. In red, the $v_0 = 3.1\mu m/s$ and in black $v_0 = 0.0\mu m/s$.

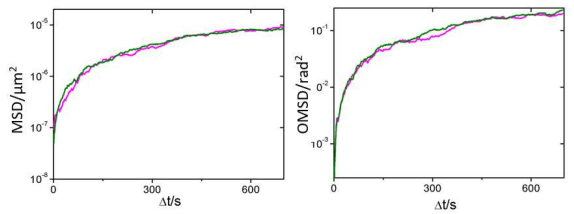

Figure 4: The corresponding MSD for $E = 10$. The particles have $v_0 = 3.1\mu m/s$ in green and $v_0 = 0.0\mu m/s$ in pink.

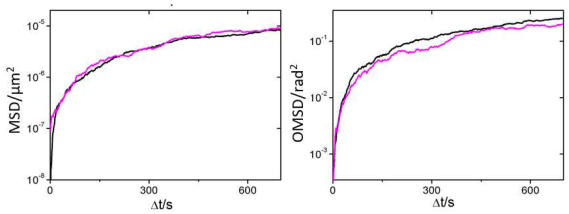

Figure 5: We compare the MSD for fields that change from $E = 0$ (in black) and $E = 10$ (in pink), for passive particles.

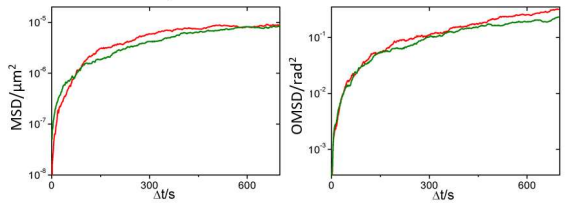

Figure 6: With $v_0 = 3.1\mu m/s$, we graph the MSD for $E = 0$ (red) and $E = 10$ (green).

4. Conclusion

The brownian dynamics for a Janus active particle in a diluted system shows the accelerated growth in the particle's displacement in field's direction.

The presence of the interaction potential in a diluted system does not change a lot the behavior. It is evident that the greatest movement in the direction of the z axis is carried out when we have the active system without the action of the external field, its mobility remains free without this external force. The system of passive particles without field is the one that has a smaller displacement.

Through the different simulations, it is observed that without applied field and with speed, the system has a higher MSD than when it is subjected to an external force or if it is a passive system. The orientational MSD works in the same way, since a plateau is reached earlier for the field system.

References

[1] Walther, A., Müller, A. *Janus particles*. Royal Society of Chemistry. **4**, 663-668 (2008).

[2] Donald L. Ermak y J. A. McCammon *Brownian dynamics with hydrodynamic interactions.* J. Chem. Phys. **69**, 1352 (1978).

[3] Howse, J. et al. *Self- Motile Colloidal Particles: From Directed Propulsion to Random Walk.* PRL, **99**, 048102 (2007).

[4] Stark, H. *Swimming in external fields.* Eur. Phys. J. **225**, 2369-2387, (2016).

[5] J. K. G. Dhont, *An Introduction to Dynamics of Colloids.* Elsevier, Amsterdam, (1996).

[6] Zottl A., Stark H.*Emergent behavior in active colloids* J. Phys.: Condens. Matter **25**, No.25 (2016).

Analysis of the implementation of obstacles in the Vicsek model.

Hector Elías de la Vega-Rosales[1] **and Francisco Alarcon**[2] *
División de Ciencias e Ingenierías, Universidad de Guanajuato,
Lomas del Bosque 103, 37150 León, Mexico.
[1]*delavegarh2018@licifug.ugto.mx*
[2]*paco@fisica.ugto.mx*

Typically, active particles are very complex systems and thus very difficult to characterize, in this work we study numerically active particles interacting with both solid obstacles and with external fields. We will show preliminary results of the interaction among the Vicsek particles and the obstacles/fields. We are capable to tailoring the direction of the field in order to modify the trapping and direction of the particles.

Keywords: Active matter, Vicsek particles, numerical simulations, heterogeneous suspensions.

1. Introduction

The active matter are systems out of equilibrium, we focus this work in self-propelled particles interacting among them. There are a lot of models which describe the interaction between self-propelled particles. The simplest one calls the Vicsek Model. This model has been used to describe a school of fishes, flocks of birds, movements of bacteria [1] or as in this case, you can study how active particles interact with both solid obstacles of different geometries and fields.

We have considered Vicsek particles in two main systems: with solid obstacles with three different collision rules [2] and with fields that align the particles locally.

2. Model and simulation details

We have worked with the Vicsek model, where we are able to control the number of particles, the size of the simulation box, thus the density of particles, the self-propelled speed, the cutoff-radio, which is the maximum distance of interaction between particles and the noise parameter which controls the alignment of the particles [1]. We have used periodic boundary conditions in all the simulations.

To start the simulation, we need to define the density of particles and the size of our simulation box, with this we can assign the number of particles in the simulation as follows

$$N = \rho L^2 \tag{1}$$

Then, we set the cutoff-radio r_c, the parameter of noise for all the particles (η). Each particle has a constant self-propel speed of v and the velocity $\mathbf{v}_i$, of the ith-particle at time t is completely determined by its direction of motion θ_i

$$\mathbf{v}_i = v(\hat{i}cos\theta_i + \hat{j}sin\theta_i) \tag{2}$$

Every time step Δt, the direction θ_i and position $\mathbf{r}_i$ of every particle is updated as follow:

1. For each i-th particle, we check for all the neighbor particles, where the j-th particle is a neighbor particle of i if $|r_i(t) - r_j(t)| \leq r_c$.
2. We compute the mean orientation θ_i^m of all the neighbor particles of the i-th particle.
3. Then, the orientation of the i-th particle at $t + \Delta t$ is given by:

$$\theta_i(t + \Delta t) = \theta_i^m + \eta\xi \tag{3}$$

where η is the noise parameter, a constant parameter between $[0 : 1]$ and ξ is a stochastic value between $[-\pi : \pi]$.

4. Each particle's position is then updated according to

$$\mathbf{r}_i(t + \Delta t) = \mathbf{r}_i(t) + \mathbf{v}_i(t + \Delta t)\Delta t \tag{4}$$

Particles positions are randomly set as the initial configuration, as well as the initial directions, which are random directions between $[-\pi : \pi]$. For each simulation shown here, the time-step is $\Delta t = 1$ the self-propel speed $v = 0.5$,the cutoff-ratio $r_c = 1$ with a box size $L = 30$.

2.1. *Solid obstacles with three different collision rules*

We have 3 different collision rules with solid obstacles:

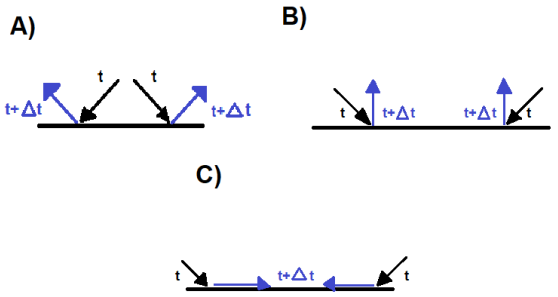

Figure 1: Types of collisions. **a)** Elastic collision, **b)** Perpendicular collision and **c)** Parallel collision.

In panel a) of Fig. 1, we have an elastic collision, similar to the light rays reflected following Snell law. In Fig. 1 panel b) the particle collides with the obstacle and it seems that it absorbs everything like a trampoline and expels it in a line perpendicular to the obstacle, whereas in Fig. 1 panel c), particles move along the surface of the obstacle.

*F.A. acknowledges support from Apoyo a la Incorporación de Nuevos PTC del Programa para el Desarrollo Profesional Docente, Tipo Superior (PRODEP) 511-6/2020-8590.

2.2. *Local fields*

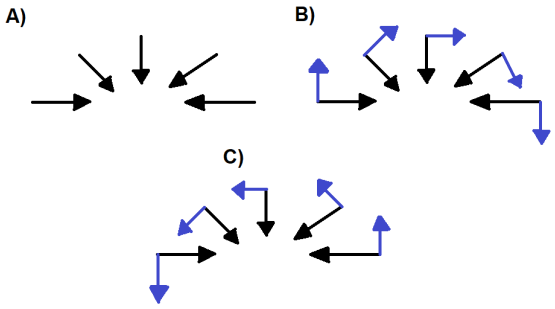

Figure 2: Types of shocks.

For this system we defined some areas on the simulation box where particles will align according to the field defined in such point. Here we need to control 3 different aspects: The number of local points, the second is the weight of poles, which it is essentially the intensity of the field. The last aspect is related to the direction of the field. With these three basic aspects we are able to control the trapping and the direction of the trapped particles

3. Results.

3.1. *Vicsek Model.*

For these simulation we have used $N = 10000$ and we tuned the noise parameter $\eta = 0.1, 0.3, 0.6$

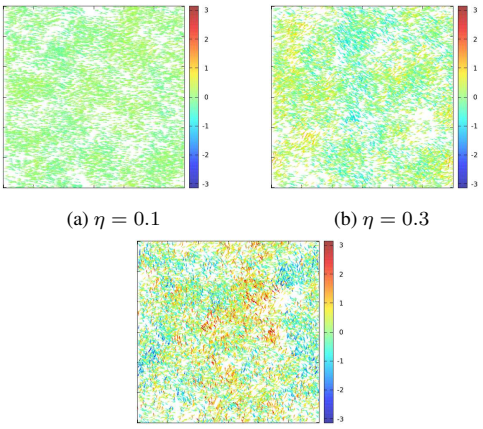

(a) $\eta = 0.1$ (b) $\eta = 0.3$

(c) $\eta = 0.6$

Figure 3: Vicsek Model.

3.2. *The restricted area.*

For these simulations we have used $N = 10000$ and we use a noise parameter equal to 0.15, the size of the restrictive area equal to 10 and the geometrical form is a square. These pictures obtained

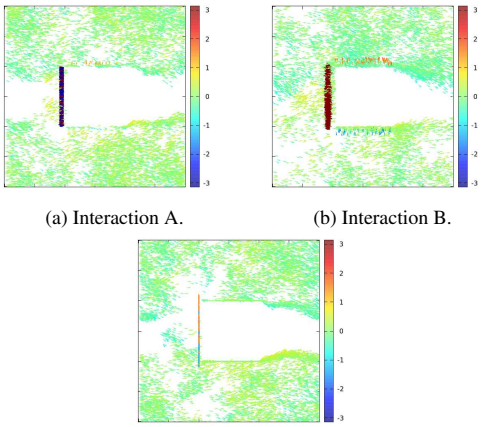

(a) Interaction A. (b) Interaction B.

(c) Interaction C.

Figure 4: Vicsek Model with restricted areas.

3.3. *Local Fields*

For these simulations we have used $N = 10000$ and we use a noise parameter equal to 0.15, each point of the field behaves as fixed Vicsek particles with higher value of alignment. The number of poles in our sum is 16 and it have around 50 particles each other and the geometrical form is a circle . The Panel **a)** on Fig. 5 is the basic case where all the field is concentrated around a circle, while in panel **b)** of Fig. 5 it is important to mention that depending on the direction of the local field, several new configurations and collective motion appears. Finally, we try to investigate the competition between closer neighbors, we put many circles at different distances to study the competition of the trapping and the alignment for different cases. In Fig. 5:

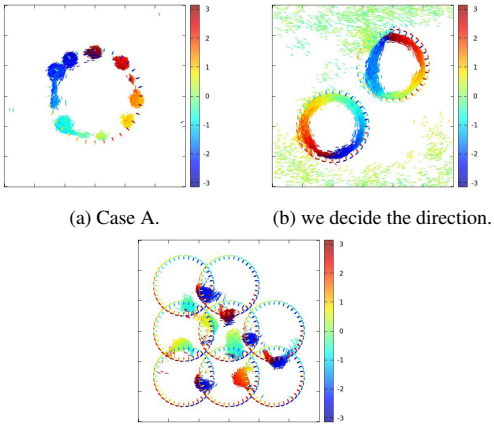

(a) Case A. (b) we decide the direction.

(c) Many circles to simulate.

Figure 5: Vicsek Model with poles of particles..

References

[1] Martinez, R., Alarcon, F., Rodriguez, D. R., Aragones, J. L., & Valeriani, C. (2018). Collective behavior of Vicsek particles without and with obstacles. The European Physical Journal E, 41(8), 1-11.

[2] Reichhardt, C. O., Drocco, J., Mai, T., Wan, M. B., & Reichhardt, C. (2011, September). Active matter on asymmetric substrates. In Optical Trapping and Optical Micromanipulation VIII (Vol. 8097, p. 80970A). International Society for Optics and Photonics.

Clustering of colloids with depletion attraction in confinement

S. López-Godoy and A. Kozina*

Instituto de Química, Universidad Nacional Autónoma de México,
Ciudad Universitaria, Mexico City, Mexico
lopez.godoy.samuel@gmail.com, akozina@unam.mx

Abstract

Colloids confined to quasi-2D have gained attention due to the possibility to verify theoretical predictions experimentally. While colloid-polymer mixtures are well studied in 3D, similar systems in 2D have not received enough attention. Therefore, in the present work a binary mixture of large and small fluorescent colloids was used to explore the effect of depletion attraction produced by small particles on large ones. Optical microscopy was used to characterize these systems. Preliminary results at low packing fractions indicate clustering of large particles. The clusters become more branched as the area fraction of large particles increases. Radial distribution functions obtained from the micrographs indicate a decrease of inter-particle distance with increasing volume fraction of small particles.

Keywords: colloids, quasi-2D, depletion attraction

1. Introduction

Colloidal suspensions are known to have rich phase behaviour depending on their volume fraction, temperature, inter-particle interactions and external forces. The simplest model to study is nearly hard-sphere colloids. The model assumes that particles are spherical and have no interactions at any distance except the one in contact where they have a steep repulsion [1]. The phase behaviour of such systems has been well studied in 3D. Hard-sphere suspensions in 2D show the phase behaviour different from that in 3D. The former has been theoretical described by KTHNY theory, which predicts solid melting via an intermediate phase called hexatic phase [2,3,4,5,6]. Hexatic phase has crystal-like orientational order but no positional order because of local particle dislocations.

Another type of interaction that have gained attention is depletion attraction. This appears in an asymmetric binary mixture of large and small particles [7]. Large particles aggregate and the volume available to small particles increases resulting in the system entropy growth. Therefore, the phenomenon is thermodynamically favourable. Previous experiments reported anomalous behaviour of depletion potential in cuasi-2D systems, where attraction was found to be stronger than expected for its 3D counterpart [8]. However, closer analysis of these systems is lacking.

In the present work, we use a binary mixture composed by large (3 μm in diameter) and small (270 nm in diameter) silica particles dispersed in water. Small particles are made fluorescent to improve their location in the system. The system is confined between two glass plates and particle positions are obtained from optical microscopy images. Resulting structure is analysed on variation of area fraction of large particles and volume fraction of small particles.

2. Methodology

Large silica particles were purchased from Bang Labs, USA. Small fluorescent particles were synthesized by the Stöber synthesis with a previous reaction between 3-aminipropyltriethoxisilane (APTES) and Rhodamine B isothiocyanate (RBITC) during 3 h at room temperature. In the Stöber synthesis ammonium hydroxide was used as a catalyst and tetraethyl orthosilicate (TEOS) was used as monomer, which was added quickly to the reaction mixture. Resulting particles were washed by sedimentation-redispersion and dried. Particle size was than characterized by static light scattering (SLS).

Stock suspensions of large and small particles were prepared at volume fraction $\phi = 6.667 \cdot 10^{-3}$, which were then mixed in different proportions. A drop of every mixture was placed on a hydrophobic microscopy slide. A hydrophobic coverslip was placed over the drop and the system was sealed with an epoxy resin while being carefully pressed. The systems were allowed to relax for 2 h before their observation under the microscope.

Optical microscopy images were taken at different relaxation times. Every set of images was analysed with IDL software where particle centres were located [9]. Using a Fortran routine that considers every image as a probable system configuration, the radial distribution function was obtained. The routine uses centre coordinates of a reference particle and correlates these data with all the other particle centres.

3. Results and discussion

It has been reported that silica particles' size depends on the rate of monomer addition: the faster is the addition, the smaller is the size [10]. Therefore, to obtain small particles, the monomer had to be added very quickly. SLS results for particles synthetized by the Stöber method show that the particles with 270 nm diameter could be obtained. On the other hand, particle observation under the fluorescent microscope revealed particles fluorescence.

The micrographs of binary mixtures show that at low volume fraction of small particles no aggregation is observed. However, when the volume fraction increases, aggregates of large particles appear. These aggregates are lineal, and when the area fraction of large particles increases, the aggregates become branched. Radial distribution function *g(r)* has been obtained for every case. The function provides information about the probability of finding a centre of particle separated by a certain distance from the centre of a reference particle. Every maximum in this function represents a high probability of finding a centre of particle at that

*Financial support from CONACyT (A1-S-21124, scholarship 1027765) and DGAPA-PAPIIT (IN100619) is gratefully acknowledged.

distance. The results obtained for these experiments show that when the volume fraction of small particles increases, the inter-particle distance characterized by the first peak of *g(r)* decreases, which implies that the particles become closer, which is consistent with the aggregates observed in the micrographs.

Moreover, an increase in the height of the first peak can be observed in some cases, which means that more particles have close neighbours in comparison with systems without small particles. This is due to the large particle clustering. Such a clustering is the result of depletion attraction. In quasi-2D every large particle has an excluded volume in which small particles cannot enter. It is important to note that the small particles are in a 3D environment, but the large particles are in a cuasi-2D environment. When excluded volumes of large particles overlap, they form 2D-agregates, and the 2D-clustering in observed.

References

[1] Pusey, P. N, Van Megen, W., Underwood, S. M., Bartlett, P., and Ottewill, R. H., Colloidal fluids, crystals and glasses, *Physica A: Statistical Mechanics and its Applications,* 176, pp. 16-27, 1991.

[2] Kosterlitz, J. M. and Thouless, D. J., Long range order and metastability in two dimensional solids and superfluids, *J. Phys. C: Solid State Phys,* 5, pp. L124, 1972.

[3] Kosterlitz, J. M. and Thouless, D. J., Ordering, metastability and phase transition in two-dimensional systems, *J. Phys. C: Solid State Phys.,* 6, pp. 1181, 1973.

[4] Halperin, B. I. and Nelson, D. R., Theory of two-dimensional melting, *Phys. Rev. Lett.,* 41, pp. 121, 1978.

[5] Nelson, D. R and Halperin, B. I., Dislocation-mediated melting in two dimensions, *Phys. Rev. B, Stat. Phys.,* 19, pp. 2457, 1979.

[6] Young, A. P., Melting and the vector Coulomb gas in two dimensions, *Phys. Rev. B,* 19, pp. 1855, 1979.

[7] Lekkerkerker, H. N. W. and Tuinier R., *Colloids and the Depletion Interaction,* Springer, Dordrecht, 2011.

[8] Cui, B., Lin, B., Frydel, D. and Rice, A., Anomalous behaviour of the depletion potential in quiasi-two-dimensional binary mixtures, *Phys. Rev. E.,* 72, pp. 021402, 2005.

[9] Crocker, J. C., Grier, D. G., Methods of digital video microscopy for colloidal studies, *J. Coll. Int. Sci.,* 179, pp. 298-310, 2996.

[10] Nozawa, K., Gailhanou, H., Raison, L., Panizza, P. Ushiki H., Sellier, E., Deville, J. P., Deville, M. H., Smart control of monodisperse Stöber silica particles: Effect of reactant addition rate on growth process, *Langmuir,* 21, pp. 1516-1523, 2005.

Clusters of sticky hard spheres: thermodynamic identification and morphology

Fernando Soto-Bustamante[1], Néstor E. Valadez-Pérez[2], Yun Liu[3,4], Ramón Castañeda-Priego[1], and Marco Laurati[5]

[1] *División de Ciencias e Ingenierías, Campus León, Universidad de Guanajuato*
Loma del Bosque 103, Lomas del Campestre, 37150 León, Guanajuato, México
sotobf2012@licifug.ugto.mx / ramoncp@fisica.ugto.mx

[2] *Facultad de Ciencias en Física y Matemáticas, Universidad Autónoma de Chiapas*
Carretera Emiliano Zapata km 8, 29050, Tuxtla Gutiérrez, Chiapas, México
nestor.valadez@unach.mx

[3] *NIST Center for Neutron Research, National Institute of Standards and Technology*
20899 Gaithersburg, Maryland, United States

[4] *Department of Chemical and Biomolecular Engineering, University of Delaware*
19716 Newark, Delaware, United States
yunliu@udel.edu

[5] *Dipartimento di Chimica & CSGI, Università di Firenze,*

50019 Sesto Fiorentino, Italy
marco.laurati@unifi.it

Abstract

Attractive particles form clusters with different sizes and shapes depending on the actual interaction between pairs of particles, but also depending on the thermodynamic state of the system. In a recent publication [Phys. Rev. Lett. **120**, 248004 (2018)] we investigated the relation between the pair interaction and the morphology of clusters of pure attractive particles by using Monte Carlo simulations. Our findings indicate that the morphology, quantified by the fractal dimension of clusters, is determined by the reduced second virial coefficient, B_2^*. However, this effective interaction is not easily obtained for any experimental system. In this contribution we present the structural properties of colloid-polymer mixtures obtained through confocal microscopy. Our results show that clustering of particles depends on the polymer concentration in terms of the overlap concentration, c_p/c_p^*. This quantity also determines the fractal dimension of clusters and other structure observables in the vicinity of the gel transition.

Keywords: colloidal clusters, phase diagram, fractal dimension

Dynamic arrest in liquids with competing interaction

Ana Gabriela Carretas-Talamante[1†] **and Magdaleno Medina-Noyola**[1*]

[1] *Instituto de Física "Manuel Sandoval Vallarta", Universidad Autónoma de San Luis Potosí, Álvaro Obregón 64, 78000, San Luis Potosí, SLP, Mexico*

[†] *gabrielacarretas@if.uaslp.mx*

[*] *medina@mail.ifisica.uaslp.mx*

Abstract

In this work we study a model of a colloidal liquid with competing short-range attractions and long-range repulsions (SALR) [1]. Employing the methodology proposed by Ruiz-Estrada, et all.[2] we are able to obtain the structural information of the system and the thermodynamic phase diagram. In order to test our structural information, we provide a comparison of the thermodynamic properties obtained with our methodology and the obtained with different approaches reported in the literature [3] [4]. For last, we compute the dynamic arrest transition lines in the framework of the self-consistent generalized Langevin equation (SCGLE) theory of colloid dynamics [5] for this colloidal model.

Keywords: ICSTCF2021, colloids, competing interactions, short-range attraction, long-range repulsion, yukawa fluid, dynamic arrest

References

[1] Ruiz-Franco, J., and Zaccarelli, E., On the Role of Competing Interactions in Charged Colloids with Short-Range Attraction, *Annu. Rev. Condens. Matter Phys.*, 12:51–70, (2020).

[2] Ruiz-Estrada, H., Medina-Noyola, M., and Nägele, G., Rescaled mean spherical approximation for colloidal mixtures, *Physica A*, 168:919-941 (1990).

[3] Archer, A.J., Ionescu, C., Pini, D., and Reatto, L., Theory for the phase behaviour of a colloidal fluid with competing interactions, *J. Chem. Phys.*, 126, 014104 (2007).

[4] Jianlan W., Yun L., Wei-Ren C.,2 Jianshu C., and Sow-Hsin C., Structural arrest transitions in fluids described by two Yukawa potentials, *Physical Review E*, 70, 050401(R) (2004).

[5] Yeomans-Reyna, L., Chávez-Rojo, M.A., Ramírez-González, P.E., Juárez-Maldonado, R., Chávez-Páez, M., and Medina-Noyola, M., Dynamic arrest within the self-consistent generalized Langevin equation of colloid dynamics. *Physical Review E*, 76(4), 041504 (2007).

[6] Archer, A.J., Pini, D., Evans, R., and Reatto, L., Model colloidal fluid with competing interactions: Bulk and interfacial properties, *J. Phys.: Condens. Matter*, 20:415106, (2008).

[7] Yun, L., Wei-Ren, C., and Sow-Hsin, C., Cluster formation in two-Yukawa fluids, *J. Chem. Phys.*, 122, 044507 (2005).

Effect of the gravitational field on the gelation in sticky colloidal dispersions

Jaime Martínez-Rivera[1,a)] **and Ramón Castañeda-Priego**[1,b)]

[1]*División de Ciencias e Ingenierías, Campus León, Universidad de Guanjuato*
Loma del Bosque 103, Colonia Lomas del Campestre, 37150 León, Guanjuato, México
[a)]*j.martinezrivera@ugto.mx*
[b)]*ramoncp@fisica.ugto.mx*

Abstract

In recent years, much effort has been done to understand the physical mechanisms that lead to colloidal gelation. Some groups claim that the frustration of the spinodal decomposition might be understood as a kind of universal route for the formation of colloidal gels in short-ranged attractive colloids [1]. However, recent experimental evidence [2] pointed out that such route may be a consequence of the competition between gravitational forces and the attractive ones between colloidal particles. Furthermore, it was found that there is a critical and effective gravitational Péclet number that clearly indicates the onset of phase separation-induced gelation. Nevertheless, this important observation has not been studied in detail at the molecular level. Then, to have a better understanding of the gravitational effects on the formation of colloidal gels, in this contribution, we have performed extensive Monte Carlo computer simulations of sticky particles under the influence of a gravitational field. The Asakura-Oosawa potential, which describes the depletion-induced attraction between colloids immersed in a bath of non-adsorbing polymers, was used to model the forces between colloidal particles [3]. We systematically analyze the effects that gravity has on the percolation, the cluster size distribution and the fractal dimension of the resulting aggregates. From this analysis and from the determination of those states where the critical gravitational Péclet number occurs, we have built a state diagram in terms of the strength of the attractive forces and the bare Péclet number. We thus report the boundary where the onset of gelation might be associated to gravity.

Keywords: Gelation, Péclet number, colloidal dispersions

References

[1] Lu, P. J., Zaccarelli, E., Ciulla, F., Schofield, A. B., Sciortino, F. and Weitz, D. A., Gelation of particles with short-range attraction, *Nature*, 453, p. 449, 2008.

[2] Kim, J. M., Fang, J., Eberle, A. P. R., Castañeda-Priego, R. and Wagner, N. J., Gel transition in adhesive hard-sphere colloidal dispersion: The role of gravitational effects, *Phys. Rev. Lett.*, 110, p. 208302, 2013.

[3] Whitmer, J. K. and Luijten, E., Sedimentation of aggregating colloids, *J. Chem. Phys.*, 134, p. 034510, 2011.

Experimental method for measuring temperature in microfluids using optical tweezers

Cecilia Romero González[1], Beatriz Morales Cruzado[2] and Francisco Gerardo Pérez Gutiérrez[3]

[1] *UASLP*
cecirog4@hotmail.com

[2] *CONACYT-UASLP*
bettiche_1102@yahoo.com.mx

[3] *UASLP*
francisco.perez@uaslp.mx

Abstract

In this work, an experimental method for measuring temperature in a microfluid using optical tweezers is proposed. The proposed method is based on the hypothesis that the relationship that exists between the kinetic energy of a trapped particle and its temperature is such that, by studying the particle's Brownian motion, the temperature of the microfluid in which it is suspended can be measured. The starting point of the project was to propose different methodologies for heating the sample, including the use of an infrared laser, exposing the sample to thermal radiation, and heating by conduction using resistors. To this moment, the results obtained show that, when heating the microfluid, the trapped particle can display an unusual behaviour, where its Brownian motion is no longer completely random and shows a tendency to make larger displacements in a single direction. Among other hypotheses, it is believed that this phenomenon may occur because the microfluid reaches a temperature that deforms the polystyrene microparticle.

*Footnotes may appear on the first page only to indicate research grant, sponsoring agency, etc. These should not be numbered but referred to by symbols, e.g. *,+. The footnote text may be produced in a small font.

Hydrodynamic correlations of trapped particles in optical tweezers

N. Palmero[1], B. Morales-Cruzado[2], Ramón Castañeda-Priego[1] and E. Sarmiento-Gomez[1]*

[1] [1]*División de Ciencias e Ingenierías, Universidad de Guanajuato, México*
normita920310@gmail.com, ramoncp@fisica.ugto.mx, esarmiento@fisica.ugto.mx

[2] *Facultad de Ingeniería, University of San Luis Potosi, Mexico*
bettiche_1102@yahoo.com.mx

Abstract

The understanding of hydrodynamic interactions in complex fluids is relevant in several branches of science. Phenomena such as hydrodynamic synchronization in either biological system (sperm, cilia, flagella), active colloidal arrays, and the dynamics of micro-swimmers can be only explained in terms of hydrodynamic coupling. In this work we report experimental results corresponding to a direct measurement of hydrodynamic interactions of two microscopic Brownian particles separated a given distance and trapped in optical tweezers. Using the positions of the two beads, we computed the cross-correlation function of displacements for different laser powers. The experimental results were compared with a theoretical model, finding a good agreement with our experiments.

*Footnotes may appear on the first page only to indicate research grant, sponsoring agency, etc. These should not be numbered but referred to by symbols, e.g. *,+. The footnote text may be produced in a small font.

Impact of the fractal dimension on the diffusion of a colloidal particle in porous confinements

Román Perdomo-Pérez[1†] **and Ramón Castañeda-Priego**[1*]

[1] *División de Ciencias e Ingenierías, Universidad de Guanajuato*
Loma del Bosque 103, Col. Lomas del Campestre, 37150, León, Guanajuato, México
[†] *r.perdomoperez@ugto.mx*
[*] *ramoncp@fisica.ugto.mx*

Abstract

The dynamical properties of particles in porous materials are affected by the complex morphology of the confinement and the distribution of the accessible volume leading to anomalous diffusion, $\langle \Delta r^2(t) \rangle \propto t^{\alpha}$ [1, 2, 3]. Recently, many efforts have been made in order to relate the anomalous diffusion with the fractal dimension of the porous matrix [4, 5]. In this context, we investigate the diffusion of a tracer particle of diameter σ_t immersed in a fractal porous environment by using Brownian dynamics simulations. The fractal matrix is made up by an array of percolating clusters with a well defined and controlled fractal dimension d_f and a specific correlation length ξ. Our findings show that tracers exhibit anomalous diffusion at $\Delta t < \frac{\xi^2}{6}$ and becomes diffusive ($\alpha = 1$) when $\Delta t > \frac{\xi^2}{6}$. Later we show that increasing the diameter of the tracer particle the effect of the fractal dimension remains in the range of ξ/σ_t corroborating the concept of self-similarity typical of fractal-like structures.

Keywords: porous media, diffusion, colloids, fractal structures

References

[1] Alcázar-Cano, N. and Delgado-Buscalioni, R. A general phenomenological relation for the subdiffusive exponent of anomalous diffusion in disordered media. *Soft Matter*, 14(48), 9937-9949.

[2] Kurzidim, J., Coslovich, D. and Kahl, G. Impact of random obstacles on the dynamics of a dense colloidal fluid. *Physical Review E*, 82(4), 041505.

[3] Spanner, M., Schnyder, S. K., Höfling, F., Voigtmann, T. and Franosch, T., Dynamic arrest in model porous media—intermediate scattering functions, *Soft Matter*, 9(5), pp. 1604-1611, 2013.

[4] Bukowski, B. C., Keil, F. J., Ravikovitch, P. I., Sastre, G., Snurr, R. Q. and Coppens, M. O. Connecting theory and simulation with experiment for the study of diffusion in nanoporous solids. *Adsorption*, 1-78.

[5] Cai, J., Luo, L., Ye, R., Zeng, X., and Hu, X. Recent advances on fractal modeling of permeability for fibrous porous media. *Fractals*, 23(01), 1540006.

Location of the gel-like boundary in patchy colloidal dispersions: rigidity percolation, structure and particle dynamics

Javier A. S. Gallegos[1†] **and Ramón Castañeda-Priego**[1*]

[1]*División de Ciencias e Ingenierías, Campus León, Universidad de Guanajuato*
Loma del Bosque 103, Col. Lomas del Campestre, 37150, León, Guanajuato, México
[†]*ja.sanchezgallegos@ugto.mx*
[*]*ramoncp@fisica.ugto.mx*

Abstract

Based on gel states identified in experiments, rigidity percolation was proposed as the precursor of colloidal gelation in adhesive hard-sphere dispersions; the onset of gelation has a particular coordination number equal to 2.4 that can be considered as the minimum number of bonds needed to form a mechanically stable network. Although this criterion was originally established to describe mechanical transitions in network-forming molecular materials [1], it worked well to explain gel formation in colloidal suspensions with isotropic short-range attractive forces [2]. Recently, this idea has also been used to account for the dynamical arrest experimentally observed in attractive spherocylinders [3]. Then, by assuming that rigidity percolation also drives gelation in spherical colloids interacting with short-ranged and highly directional potentials, we locate the thermodynamic states where gelation seems to occur in dispersions made up of patchy colloids. We apply the so-called bond-bending analysis to determine the fraction of floppy modes at some percolating clusters. This analysis confirms that the coordination number condition is a good approximation to determine those percolating clusters that are either mechanically stable or rigid. Finally, by using dynamic Monte Carlo computer simulations, we calculate both the mean-square displacement and the intermediate scattering function at and in the neighborhood of the gel-like states.

Keywords: colloids, gels, rigidity percolation

References

[1] He H. and Thorpe M. F., Elastic Properties of Glasses, *Physical Review Letters*, 54, pp. 2107-2110, 1985.

[2] Valadez-Pérez Néstor E., Liu Yun, Eberle Aaron P. R., Wagner Norman J., Castañeda-Priego Ramón, Dynamical arrest in adhesive hard-sphere dispersions driven by rigidity percolation, *Physical Review E*, 88, p. 060302, 2013.

[3] Murphy Ryan P., Hatch Harold W., Mahynski Nathan A., Shen Vincent K. and Wagner Norman J., Dynamic arrest of adhesive hard rod dispersions, *Soft Matter*, 48, pp. 709-726, 2020.

Mesoscopic dynamics of a virus in a solvent interacting with different surfaces

J.I. Sánchez Morán[1] **and F. Alarcon**[2*]
Universidad de Guanajuato Campus León, División de Ciencias e Ingenierías
Lomas del Bosque 103, Lomas del Campestre, 37150 León, Gto.
[1] *sanchezmj2018@licifug.ugto.mx*
[2] *paco@fisica.ugto.mx*

In this work we will study the dynamics of a virus immersed in a flow which is confined by flat walls or walls with posts attached to them. The stiffness and the distribution of the posts plays a key role in the adsorption of the virus, because posts interact with the virus in two ways, one short range entropic interaction and by long and short hydrodynamic interactions. Both interactions are tuned by the parameters of the posts.

Keywords: DPD, Confined virus, Fluid Dynamics, LAMMPS

1. Introduction

Coarse-grained models are a great tool for studying complex systems on larger time and length scales than, for example, those used in full atomistic molecular dynamics [1]. Dissipative Particle Dynamics (DPD) is one of these techniques and it is widely used to study the dynamical and rheological properties of complex fluids. We can study larger length scales because in this model a bead represents a group of atoms, from a small molecule to proteins. Additionally, larger time scales are reached since the beads are subject to soft repulsive interactions thus a larger Δt can be used.

Understanding the behavior of viruses in fluids and how they interact with surfaces is an interesting problem that can potentially lead to many applications in health.

In previous works, DPD has been used to study biofilm formation and growth on dynamically reconfigurable surfaces [2] and under hydrodynamic stress [3]. Here we show a study of different surfaces interacting with virus embedded in an explicit solvent.

2. Theoretical Background

DPD is a simulation technique which assumes a set of interacting particles whose time evolution follows Newton's equations of motion

$$\boldsymbol{F_i} = m_i \frac{d\boldsymbol{v_i}}{dt}, \quad \boldsymbol{v_i} = \frac{d\boldsymbol{r_i}}{dt}, \tag{1}$$

with particles mass equal to 1 in order to simplify the equations. The total force consists of a conservative force, a dissipative force and a random force:

$$\boldsymbol{F_i} = \sum_{i \neq j} (\boldsymbol{F}_{ij}^C + \boldsymbol{F}_{ij}^D + \boldsymbol{F}_{ij}^R), \tag{2}$$

each one of them is pairwise additive and the sum takes into account all particles within a cutoff radius r_c. The forces are shown below

$$\boldsymbol{F}_{ij}^C = \begin{cases} a_{ij}(1 - r_{ij})\hat{\boldsymbol{r}}_{ij} & r_{ij} < r_c \\ 0 & r_{ij} \geq r_c \end{cases} \tag{3}$$

$$\boldsymbol{F}_{ij}^D = -\gamma w^D(r_{ij})(\hat{\boldsymbol{r}}_{ij} \cdot \boldsymbol{v}_{ij})\hat{\boldsymbol{r}}_{ij} \tag{4}$$

$$\boldsymbol{F}_{ij}^R = \sigma w^R(r_{ij})\theta_{ij}\hat{\boldsymbol{r}}_{ij}. \tag{5}$$

In the conservative force, $\boldsymbol{r}_{ij} = \boldsymbol{r}_i - \boldsymbol{r}_j$ and a_{ij} is the maximum repulsion between particle i and particle j. In the dissipative force, $\boldsymbol{v}_{ij} = \boldsymbol{v}_i - \boldsymbol{v}_j$ and w^D is a weight function that depends on r and vanish for $r > r_c$. Finally, in the random force, θ_{ij} is a random variable with $\langle\theta_{ij}(t)\rangle = 0$ and $\langle\theta_{ij}\rangle$. [4]
In addition, the dissipative and random forces are subjected to the following constraints

$$w^D(r) = [w^R(r)]^2, \quad \sigma^2 = 2\gamma k_B T \tag{6}$$

such constraints guaranty the explicit description of the hydrodynamic interactions. [5]

3. Models

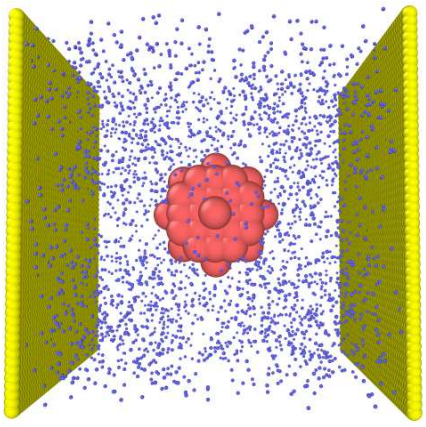

Figure 1: Model with flat walls. A virus of diameter $3r_c$ immersed in a fluid confined by two walls. Yellow beads represent the walls, red beads are the virus and blue beads are the solvent. Note that all beads have the same interaction range, size was chosen just for clarity of the snapshot.

*F.A. acknowledges support from Apoyo a la Incorporación de Nuevos PTC del Programa para el Desarrollo Profesional Docente, Tipo Superior (PRODEP) 511-6/2020-8590.

In this work we study two different models. The first one consists of a small virus immersed in a fluid confined by two fixed flat walls. The volume of the simulation box is $L \times L \times L = (10r_c)^3$ with bead number density of $\rho = 3r_c^{-3}$ without considering the walls' beads. The virus has a diameter of $3r_c$ and contains 123 beads. This model is shown in figure 1.

In order to maintain its spherical shape the beads were bonded to their closest neighbors by a harmonic force

$$\boldsymbol{F}_{ij}^{b} = -k(r_{ij} - r_0)\hat{\boldsymbol{r}}_{ij} \tag{7}$$

where k is a bond stiffness and r_0 is the equilibrium bond length. For our model the parameters are: $r_c = 1$, $k = 200$, $r_0 = 0.3$, $a_{13} = a_{23} = 10$, $a_{33} = 0$ and $a_{ij} = 30$ for the remaining combinations.

The second model adds post to the walls. The posts are arranged in a 10x10 square lattice and are made of 8 beads each. The beads are also bonded by a harmonic force so, unlike the walls, the posts are not fixed. The arrangement is shown in figure 2.

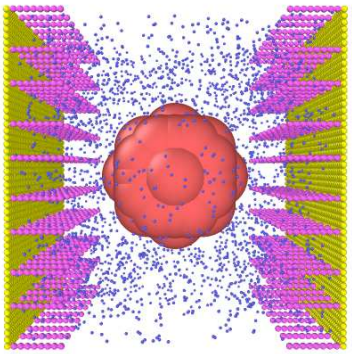

Figure 2: Second model. An array of 10x10 posts is attached to the walls. Each post is made of 8 beads. Yellow beads represent the walls, pink beads represent the posts, red beads are the virus and blue beads are the solvent. Note that all beads have the same interaction range, size was chosen just for clarity of the snapshot.

The parameters for this model are $r_c = 1$, $k_v = 200$, $k_p = 500$, $r_{0v} = r_{0p} = 0.3$, $a_{13} = a_{14} = a_{23} = a_{24} = 10$, $a_{34} = 15$, $a_{33} = 0$ and $a_{ij} = 30$ for the remaining combinations. The v subscript indicates parameters related to the virus while the p subscript indicates parameters related to the posts attached to the walls. Both models were simulated by using LAMMPS. LAMMPS is a classical molecular dynamics simulation code with a focus on materials modeling. [6]

4. Conclusions

We have developed a numerical framework to tailoring surfaces that avoid virus adsorption. Such surfaces are modified just geometrically and taking into account both direct steric repulsion and hydrodynamic interactions modified by the structures of the posts. In our preliminary results we have study the adsorption of the virus on the surfaces in terms of the stiffness of the posts and its spatial distribution on the walls.

References

[1] Frenkel, D., Smit, B., and Ratner, M. A., *Understanding molecular simulation: from algorithms to applications*, Vol. 2, San Diego: Academic press., 1996.

[2] Liu, Y., and Balazs, A. C. , Modeling biofilm formation on dynamically reconfigurable composite surfaces, *Langmuir*, 34(4), pp. 1807-1816, 2018.

[3] Jara, J., Alarcón, F., Monnappa, A. K., Santos, J. I., Bianco, V., Nie, P., Ciamarra, M. P., Canales, Á., Dinis, L., López-Montero, I., Valeriani, C. and Orgaz, B., Self-Adaptation of Pseudomonas fluorescens Biofilms to Hydrodynamic Stress, *Frontiers in microbiology*, 11, pp. 3460, 2021.

[4] Groot, R. D., and Warren, P. B., Dissipative particle dynamics: Bridging the gap between atomistic and mesoscopic simulation, *The Journal of chemical physics*, 107(11), pp. 4423-4435, 1997.

[5] Espanol, P., Warren, P., Statistical mechanics of dissipative particle dynamics, *EPL (Europhysics Letters)*, 30(4), pp. 191, 1995.

[6] Plimpton, S., Fast Parallel Algorithms for Short-Range Molecular Dynamics, *J Comp Phys*, 117, pp. 1-19, 1995

MESOSCOPIC SIMULATION OF A VIRUS BY DISSIPATIVE PARTICLE DYNAMICS

K. Gonzales-Flores,[1] ***R. Castañeda-Priego,**[1] **and F. Alarcon** [1] †

División de Ciencias e Ingenierías, Campus León, Universidad de Guanajuato, Lomas del Campestre, 37150 León, Guanajuato, México

[1] *k.gonzalesflores@ugto.mx*

[2] *ramoncp@fisica.ugto.mx*

[3] *paco@fisica.ugto.mx*

Abstract

The 2019-nCoV pandemic caused by the severe acute respiratory syndrome coronavirus 2 (SARS-CoV-2) has been responsible for a global outbreak that has resulted in the death of approximately 3 million people around the world. According to numerous and recent investigations, the most effective route for the spread of Covid-19 is due to the airborne transmission through, for example, saliva droplets. Thus, this work aims to study the hydrodynamic transport of a virus model to understand how its diffusion through a continuum medium, such as water, is affected by the hydrodynamic interactions and to associate the results with the degree of contagion of the virus. We have carried out mesoscopic simulations by using Dissipative Particle Dynamics (DPD) where both fluid and viral capsid are modeled explicitly. We apply such methodology by using the Large-scale Atomic/Molecular Massively Parallel Simulator (LAMMPS) [1] and the input files were generated by the Moltemplate platform [2].

Keywords: SARS-CoV-2,DPD,Moltemplate,LAMMPS

1. Introduction

The coronavirus disease 2019 (COVID-19) has caused a global outbreak that exposes the impact of viruses on our daily live as infectious agents [3, 4], this current situation has brought promising areas for future research such as physical virology that proposes the study of the mechanical properties [5, 6], thermodynamic properties and hydrodynamic properties of viral capsids to understand the infection process of viruses [7].

Biological complex systems need numerical simulations to understand from a meso and microscopical point of view different properties of viruses. Thus, the objective of this work is to study the hydrodynamic transport of viruses by implementing the mesoscopic simulation method of dissipative particle dynamics (DPD) [8].

The dynamic analysis of the diffusion and transport of these viruses such as colloids is essential to understand the transport mechanisms through secretion droplets that allow an eventual contagion outbreak that may change according to conditions of the environment [9, 10].

2. Model

2.1. DPD Algorithm

DPD particles interact with an additive soft potential in pairs where the total force exerted on particle i by particle j will be the sum of 3 pairwise forces: the conservative force, the dissipative force and the random force given by [8, 11]

$$\bar{F}_{ij}^{C} = A_{ij}\omega_C(r_{r_{ij}}\hat{e}_{ij}), \tag{1}$$

$$\bar{F}_{ij}^{D} = -\gamma\omega_D(r_{ij})(\hat{e_{ij}}.\bar{v_{ij}})\hat{e_{ij}}, \tag{2}$$

$$\bar{F}_{ij}^{R} = \sigma\omega_R(r_{ij})\hat{e}_{ij}\zeta_{ij}, \tag{3}$$

where:

$$\omega_C(r_{ij}) = \left(1 - \frac{r_{ij}}{r_c}\right), \tag{4}$$

where a_{ij} represents the maximum repulsion between two particles [12], γ is the coefficient of friction, ζ_{ij} is a symmetric white noise function, σ is the noise amplitude of the random signal. The terms $\omega_D(r_{ij})$ and $\omega_R(r_{ij})$ in equations 2 and 3 respectively are weight functions distance dependent[8].

By rewriting the Newton's second Law of motion of the DPD forces, we obtain a set of Langevin equations equivalent to the Fokker-Planck equation [12, 13]

$$\partial_t\rho(r,p;t) = L_C\rho(r,p;t) + L_D\rho(r,p;t), \tag{5}$$

where L_C is the Liouville operator and the operator L_D contains the random and dissipative forces. The steady-state solution is canonical ensemble (NVT) under these conditions [12]:

$$\omega_R(r) = \omega_D^{1/2}(r), \tag{6}$$

$$\sigma = (2k_BT\gamma)^{1/2}, \tag{7}$$

where (7) is the fluctuation-dissipation theorem for the DPD method [11] that allows with eq. (6) the explicit description of the hydrodynamic interactions [14].

2.2. Modeling Viral Capsid

To study the dilute regime of a virus suspension, we have carried out systematic simulations of a single virus immersed in water in bulk, with periodic boundary conditions. Both the solvent and the virus are represented by DPD particles.

The initial model of the virus was built with DPD particles to form rigid spheres of radii $10r_c$, $5r_c$, $3r_c$ y $2r_c$, thus composed by 1239, 305, 112 and 50 DPD beads respectively (see Fig. 1), where we use the cutoff radius as our unit of length, $r_c = 1$.

*G.R.V. acknowledges support provided by CONACYT for the development of this research, CVU:1047374

†F.A. acknowledges support from Apoyo a la Incorporación de Nuevos PTC del Programa para el Desarrollo Profesional Docente, Tipo Superior (PRODEP) 511-6/2020-8590.

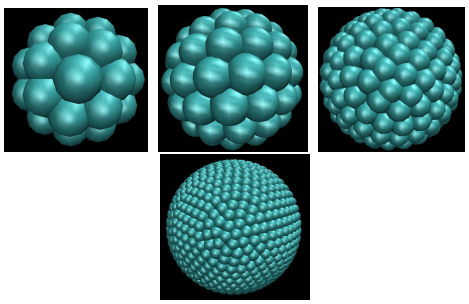

Figure 1: Rigid body models of the viral capsid with different radius constructed with LAMMPS.

3. Results and discussion

3.1. Tools

To characterize the dynamics of the virus in a solvent, the mean square displacement (MSD) has been calculated by

$$MSD(t) =< [x(t) - x(0)]^2 >, \quad (8)$$

where $MSD \propto t^{\beta}$, if $\beta = 2$ is a ballistic regime and if $\beta = 1$ it is a diffusive regime . When the system evolves to a diffusive regime, the diffusion constant is defined as [15]

$$D = lim_{t\to\infty} \frac{1}{2nt} < [x(t) - x(0)]^2 >, \quad (9)$$

where n is the system dimension.

3.2. Diluted system

The first results found are related to the effect of virus size and temperature. We have carried out simulattion with box length $L = 14$, $\rho = 3$, $\gamma = 4.5$ and $\sigma = 3$.

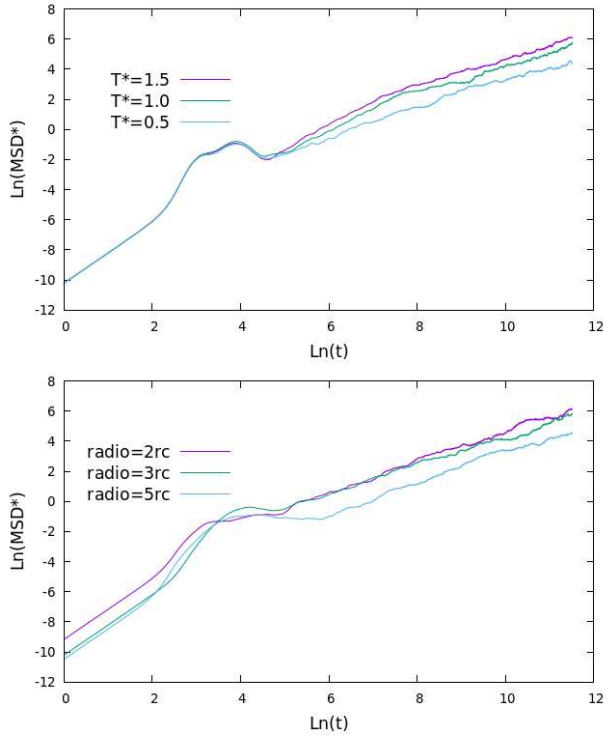

Figure 2: a) For the virus radius=$3r_c$ the diffusion constant $D^* = 7.16 \times 10^{-4}$ to $T = 1.5$, 4.48×10^{-4} to $T = 1$ and 1.38×10^{-4} to $T = 0.5$. b) The diffusion constant $D^* = 6.48 \times 10^{-4}$ to virus radius $= 2r_c$, 5.30×10^{-4} to virus radius $= 3r_c$ and 1.68×10^{-4} to virus radius $= 5r_c$

Diffusion of the viral capsid increases with the temperature (see Fig. 2 a), but when the capsid size was increased, the diffusion decreased (see Fig. 2 b). The solvation effect of the solvent with the virus was also studied, however the results (not shown here) showed that viscosity does not modify the diffusion of the virus at least for the values of viscosity studied here.

4. Conclusions

The use of rigid sphere models allowed us to study the general transport properties of a virus without detailing the degrees of freedom of the protein capsid. This helps us to obtain the minimum ingredients necessary to understand the spread of viruses, such as geometry and temperature.

The study of diffusion plays an important role in the transport mechanisms of a virus for being related to size and may be associated with outbreaks of infection through the temperature of the medium [16]. Thus, we can conclude that our numerical approach is consistent to experimental results obtained by Dbouk et al., 2021 and Olmsted et al. 2001 [9, 17].

References

[1] S. Plimpton, Fast Parallel Algorithms for Short-Range Molecular Dynamics, *J. Comp Phys*, Vol. 117, pp. 1-19,(1995). https://www.lammps.org/

[2] AI. Jewett , D. Stelter, J. Lambert, SM. Saladi, OM. Roscioni, M. Ricci, L. Autin, M. Maritan, SM. Bashusqeh, T. Keyes, RT. Dame, J. Shea, GJ. Jensen, DS. Goodsell, Moltemplate: A Tool for Coarse-Grained Modeling of Complex Biological Matter and Soft Condensed Matter Physics, *J. Mol. Biol.*, Vol. 433(11):166841, (2021). https://doi.org/10.1016/j.jmb.2021.166841

[3] R. Xu , B. Cui, X. Duan, P. Zhang, X. Zhou and Q. Yua, Saliva: potential diagnostic value and transmission of 2019-nCoV, *International Journal of Oral Science*, 12:11, pp. 1-3 ,(2020).

[4] A. Yu, A. Pak, P. He, V. Monje, L. Casalino, Z. Gaieb, A. Dommer, R. Amaro, and G. Voth, A Multiscale Coarse-Grained Model of the SARS-CoV-2 Virion, *Biophysical Journal*, Vol. 120, pp. 1–8, (2021).

[5] A. Zlotnick, Viruses and the physics of soft condensed matter, *PNAS.*, vol. 101 (44), pp. 15549 –15550, (2004).

[6] W. Roos , R. Bruinsma and G. Wuite, *Physical virology*, Nat. Rev. Phys., 6, 733-743 (2010).

[7] O. Malekahmadi, A. Zarei, M. Esfahani, M. Hekmatifar, R. Sabetvand, A.Marjani and Q. Bach, Thermal and hydrodynamic properties of coronavirus at various temperature and pressure via molecular dynamics approach, *Journal of Thermal Analysis and Calorimetry*, Vol. 143, pp. 2841–2850, (2021).

[8] P. Groot and P. Warren, Dissipative particle dynamics: Bridging the gap between atomistic and mesoscopic simulation, *J. Chem. Phys.*, Vol. 107, pp. 4423, (1997).

[9] T. Dbouk, and D. Drikakis, Fluid dynamics and epidemiology: Seasonality and transmission dynamics,*Phys. Fluids*, Vol. 33, pp. 021901, (2021).

[10] P. Corstjens, W. Abrams and D. Malamud, Saliva, and viral infections, *Periodontology* 2000, Vol. 70, pp. 93–110, (2016).

[11] P. Nikunen, M. Karttunen, and I. Vattulainen, How would you integrate the equations of motion in dissipative particle dynamics simulations?, *Computación. Phys. Comun.*, Vol. 153, pp. 407-423 (2003).

[12] P. Español and P. Warren, Statistical Mechanics of Dissipative Particle Dynamics, *Europhys. Lett.*, Vol. 30 (4), pp. 191-196, (1995).

[13] C. Li, X. Fu, W. Zhong, and J. Liu, Dissipative Particle Dynamics Simulations of a Protein-Directed Self-Assembly of Nanoparticles, *ACS Omega*, Vol. 4, pp. 10216-10224, (2019).

[14] P. Hoogerbrugge and J. Koelman, Simulating Microscopic Hydrodynamic Phenomena with Dissipative Particle Dynamics, *Europhys. Lett.*, 19 (3), pp. 155-160 (1992).

[15] S. Albaladejo, M. Marqués, and J. Sáenz, Light control of silver nanoparticle's diffusion, *OPTICS EXPRESS*, Vol. 19 (12), pp. 11472, (2011).

[16] N. Granik, L. Weiss, E. Nehme, M. Levin, M. Chein, E. Perlson, Y. Roichman, and Y. Shechtman, Single-Particle Diffusion Characterization by Deep Learning, *Biophysical Journal*, 117, 1–8 (2019).

[17] S. Olmsted, J.Padgett, A. Yudin, K. Whaley, T. Moench, and R. Cone, Diffusion of Macromolecules and Virus-Like Particles in Human Cervical Mucus, *Biophysical Journal*, Vol. 8, pp. 1930 –1937, (2001).

Modeling the dynamics of tracer particles in hydrogels by means of random walkers under confinement

S.M. Hernández-Hernández[1], Norma Caridad Palmero Cruz[2] and E. Sarmiento-Gómez[2]*

[1] *Preparatoria 2 de Octubre de 1968, Benemérita Universidad Autónoma de Puebla*
Calle Benito Juárez N. 51-B, Col. Concepción Gpe. Mayorazgo 72450 Puebla, México
sol.hernandezher@correo.buap.mx

[2] *División de Ciencias e Ingenierías, Universidad de Guanajuato*
Lomas del bosque 103,37150 León, México
e.sarmiento@ugto.mx

Abstract

The purpose of the current study is to model the dynamics of tracer brownian particles in complex fluids, such as interpenetrating polymer network hydrogels and wormlike micelles, using random walkers confined in a two-dimensional box of several sizes. The ensemble of different sizes was established using right skewed distribution and the mobility of the walkers was limited by confinement conditions in the walls of the boxes. We found that the width of the distribution of cage sizes produces a smooth transition between the dynamical regimes usually found in confined brownian particles. This effect has been reported in microrheological experiments, and our results give an insight of its origin, finding that the distribution of cages for a wide distribution resembles the experimental distribution of mesh sizes.

Keywords: random walk, confined conditions, MSD.

Non-equilibrium relaxation and aging of the dynamics in a dipolar fluid quenched towards the glass transition

R. Peredo-Ortiz[1], **L.F. Elizondo-Aguilera**[2] **and M. Medina-Noyola**[3*]
Instituto de Física "Manuel Sandoval Vallarta" Universidad Autónoma de San Luis Potoí
Av. Manuel Nava #6, Zona Universitaria, C.P. 78290
[1]*rperedo@if.uaslp.mx*
[2]*luisfer.elizondo@gmail.com*
[3]*medina@mail.ifisica.uaslp.mx*

Abstract

The developed non-equilibrium self-consistent generalized Langevin equation theory for the dynamics of liquids of non-spherically interacting particles [J. Phys. Chem. B **120**, 7975 (2016)] is applied for the description of the irreversible relaxation in a dipolar liquid thermally and mechanically constrained to approach different glassy states. Specifically, we consider a dipolar hard-sphere fluid in an instantaneous quench (or a compression) at $t_w = 0$ from full equilibrium conditions towards different non-ergodic transitions. Qualitative distinct scenarios are predicted by the theory for the time evolution of the system after quenching ($t_w > 0$), depending on both the kind of transition approached and the specific features of the protocol of fabrication of a glassy state.

Keywords: ICSTCF2021, dipolar fluid, Non-equilibrium, NE-SCGLE

1. Some comments

The theoretical framework of the Non-Equilibrium Self Consistent Generalized Langevin Equation (NE-SCGLE) has been applied to monodisperse colloidal systems with spherically symmetric pair potential interaction. The prominent results obtained allow us to describe non-equilibrioum arrest diagrams for soft repulsive spheres[1], for particles with attractive interactions[2] or for a mixture of repulsive particles[3]. For particles with dipolar interaction, where the pair potential depends in the position and the orientation of their permanent dipole moment, an extension to NE-SCGLE has been developed[4].

For the dipolar hard sphere colloid can get different kind of dynamic arrest given that the particles a be constrained to move in a traslational or a rotational deeegre of freedom. *A priori* we can imagine four different kinds of arrest: 1) Full ergodic phase with infinite localization length which can be well determined by the equilibrioum verision of the present theoretical framework[5], 2) Fully non-ergodic phase where the traslational and rotational localization length is finite, this means that the particles are frozen in a particular position and orientation, 3) a mixed state with the traslational localization length finite yand the rotational infinite, in this case the particles are constrained to remain in a given postion but its rotational degree of freedom keeps evolving freely, and 4) a mixed state with the rotational degree of freedom finite and the traslational infinite.

In this poster we show some of the results of the study of hard spheres with dipoles. The complete discussion of this work is in the evaluation process.

2. Bibliography

[1] L. E. Sánchez-D´az, P. E. Ramírez-González and M.Medina-Noyola, Phys. Rev. E87, 052306 (2013)

[2] J.M. Olais-Govea, L. López-Flores, and M. Medina-Noyola,J. Chem Phys.143, 174505 (2015).

[3] E. Lázaro -Lázaro, J. A. Perera-Burgos, P. Laermann, T. Sentjabrskaja, G. Pérez- Angel,M. Laurati, S.U. Egelhaaf, M. Medina-Noyola, Th. Voigtmann, R. Castañeda-Priego and L. F. Elizondo-Aguilera,Phys. Rev. E99, 042603 (2019)

[4] L.F. Elizondo-Aguilera, E.C. Cortés-Morales, P.F. Zubieta-Rico, M. Medina-Noyola, R. Castañeda-Priego, Th. Voigtmann and G. Pérez- Angel,Soft Matte r16170 (2020)

[5] L. Yeomans-Reyna,et al.,Phys. Rev. E76, 041504 (2007).

*Laboratorio Nacional de la Ingeniería de la Materia Fuera del Equilibrio

On the reinforcing effect of solid inclusions in colloidal gels

Claudia Ferreiro-Córdova, [1] **Giuseppe Foffi,** [2] **Olivier Pitois,** [3]**, Chiara Guidolin,** [2] **Maxime Schneider** [2] **and Anniina Salonen**[2]

[1] *Tecnologico de Monterrey, Escuela de Ingeniería y Ciencias, Querétaro, Mexico*
claudia.ferreiro@tec.mx

[2] *Université Paris-Saclay, CNRS, Laboratoire de Physique des Solides, 91405, Orsay, France*

[3] *Université Gustave Eiffel, Ecole des Ponts ParisTech, CNRS, Laboratoire Navier, F-77447 Marne-la-Vallée, France*

Abstract

The mechanical properties of soft materials can be altered significantly by adding solid inclusions, here the microscopic properties of the inclusions play a key role in the behaviour of the composite material. In this work we explore, with simulations and experiments, how the mechanical properties of colloidal gels are modified by non interacting spherical inclusions. By exploring different total packing fractions ($0.3 \leq \phi_T \leq 0.6$), particle sizes and relative concentration of inclusions, we found that the elastic properties vary in a highly non-trivial way as a result of the interactions between the gel backbone and the inclusions. In particular, at total volume fractions $\phi_T < 0.6$ the addition of inclusions leads to a weak stiffening of the material, but remarkably at $\phi_T = 0.6$ the effect of the inclusions becomes strongly size dependent. For the latter, the composite material stiffens considerably if the size of the inclusions is similar to the average size of the gel particles. This is a result of the effect of the inclusions, they can change the structure of the gel backbone and the average interactions, as the gel-inclusion interactions are weaker than the gel-gel interactions. Our results provide guidance for the control over the mechanical properties of colloidal gels using inclusions.

Keywords: ICSTCF2021, colloidal gels, composite materials, mechanical properties

Phase diagram of polymer brushes with mobile attachment points in a good solvent calculated with the modified expanded ensemble method

B.F. Faria* **and A. Vishnyakov**

Skolkovo Institute of Science and Technology
Moscow, Russia
Bruna.Faria@skoltech.ru

Abstract

We explore the phase diagram of "mobile polymer brushes" (MB): the polymer molecules are not chemically bound to the particle surface but rather are adsorbed by one end; the sorption is too strong for a chain to desorb and diffuse into the solution, but weak enough so that the polymer heads can move along the surface. In a good solvent, the prevailing forces in the system (apart from the attraction between the adsorbed head and the surface) originate from steric repulsion between the individual chains. Here we explore MB systems free energy phase diagram with Monte Carlo and dissipative particle dynamics simulations using expanded ensemble techniques that we modify to make it more suitable to polymers. Expanded Ensembles are employed to calculate the excess chemical potential μ_{ex} of the polymer as a function of the surface density ρ_s, polymer length N, and excluded (effective) volume V_{ex} of the segment. The thermodynamic properties are manifested in structural features, such as brush height, chain radius of gyration, and radial distribution function between the chains. As a practical application, this work provides a way to evaluate the free energy, consequently optimizing artificial systems composed of polymers such as polymer brushes composites.

Keywords: Polymer Brush, Dissipative Particle Dynamics, Monte Carlo, Expanded Ensembles

1. Introduction

Understanding polymer adsorption at a solid-liquid interface is a subject of great technological importance having excellent applicability interest, such as optimizing surface treatments, colloids stabilization, improving chromatography methods, and oil recovery [1]. Then, polymer brushes (PB) systems present a significant interest growth once it is composed of polymers chains anchored to the surface: flat, curved, nanoparticles, and so on[2]. So, the free energy evaluation and chemical potential are essentials in generating optimized PB systems [3].

The chemical potential μ is crucial to investigate the phase equilibrium for polymeric systems. Different methods were proposed to obtain chemical potentials, such as: the particle insertion (Widom) method [4], the inverse-Widom method [5], the continuum configurational-bias (CCB) method as an extension of Widom method [6], the incremental chemical potential method [7], and expanded ensembles [8] here the bead interaction parameter is tuning gradually according to a couple and decouple process. Although time-consuming, it overcomes the main drawbacks of the other methods being applied to high densities and long chains, nonideal systems. Also, it gives free energy with high accuracy and low statistical error and can be used to investigate the conformational transitions caused by environmental changes, for instance. Consequently, this method has become one of the most important methods to calculate chemical potentials.

Finally, the polymers brushes and their adsorption process require attention, and its free energy dependence of density remains unclear. In this work, we used DPD model and MC simulations in an expanded ensemble to obtain PB chemical potential dependence of density, polymerization degree and excluded (effective) volume. Also, the structural properties were investigated. Here, we provide a way to describe PB systems and their chemical dependence. As a practical application, this work opens the doors to optimize artificial systems composed of polymers.

2. Material and Methods

Here we explored the MBs formed by polymer chains with different lengths (number of monomers), from $N = 10$ to $N = 99$. The monomers were modeled as soft beads that interacted with each other via harmonic repulsion common in dissipative particle dynamics (DPD) $E_{ij}(r) = \frac{1}{2}a_{ij}(r-R_c)^2$ when $r < R_c$, where a characterizes the repulsion strength, R_c is the effective diameter [9]. The beads of the same chain were bonded by harmonic bonds with a fixed length of $0.8R_c$. The first bead was attached to the surface: its normal coordinate z was fixed to 0. The chains were not allowed to cross the $z = 0$ plane, and periodic boundary conditions were applied in the lateral dimensions. The lateral density of the polymers varied from $0.0028R_c^{-2}$, then for this low density, the chains hardly interact with each other making, so to say, "ideal 2D polymer gas" to ¼. The system size was $60x60x100R_c^3$. The absence of explicit attraction between the beads corresponds to very good solvent conditions, so for long polymer chains, each bead (segment) experiences a steric repulsion from each other. We also examined the excluded volume effect by varying the repulsion parameter a from 100 to 500 kT/R_c.

Starting from a random configuration, we applied DPD with the LAMMPS package to reach equilibrium. To calculate the chemical potential of the chain, we modified the expanded ensembles method [8]. To the system of chains, a trial chain was added. The beads of the trial chain interacted with each other via harmonic repulsive and bond potentials. The interactions of the beads trial chain with the other beads were scaled, that is, multiplied by the vector of weights $\boldsymbol{\lambda}_i = [\lambda_{i1},\ldots, \lambda_{iN}]$. i in such an equation refers to the "state" or the ensemble. The beads experience trial displacements according to the Metropolis algorithm. In addition to the standard Metropolis moves, an ensemble change trial move was introduced: it changed the

* Computations were carried out at Zhores supercomputer facilities provided through the Skolkovo foundation [10].

system state (or the ensemble) by changing the vector of weights. The difference between the standard expanded ensemble procedure and our new modified method is that instead of a single weighting factor λ_i that scaled all interactions of the trial molecule with the environment, we introduced a matrix. In the most primitive case λ_{ij} equal 0 or 1, and the weight matrix Λ has a size of $(N+1)\times N$. Correspondingly, $\lambda_{0j} = 0$ and $\lambda_{Nj} = 1$. From the frequency of observing each state i (denoted as p_i) we can calculate the chemical potential of the chain in the system. In order to flatten the frequency histogram, we introduced a biasing vector η_i, as usually done in the expanded ensemble. When the state N is reached, the trial chain becomes indistinguishable from other chains, and another trial move is performed as a random trial chain switch. The chemical potential of this scheme is illustrated in Figure 1.

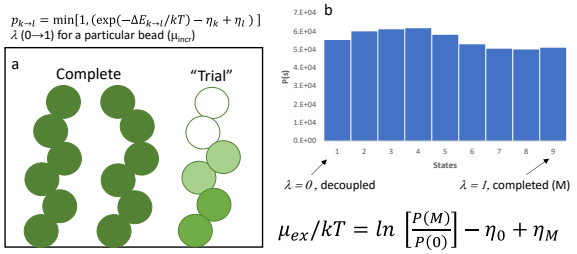

Figure 1. (a) schematics of the expanded ensemble method adopted to polymers. (b) example of frequency histogram. Bottom right: Calculation of the excess chemical potential.

3. Results

Figure 2 shows the probability density distributions for the radius of gyration of an individual chain and the brush height for $N = 98$ (the longest chain we considered) as a function of the lateral density. Certainly, the brush height growth and the radius of gyration gradually decreases with the density, which signifies the effective repulsion between the chains. Interestingly, the lateral distribution of the heads showed absolutely no short-range order, even at the highest densities. The lateral radial distribution functions showed a repulsion most visible at the middle surface densities that almost vanished at the lowest and highest densities. We refer to the structural behavior to a gradual transformation from "polymer solution" to "polymer melt". We observed that the excluded volume (V_{ex}) does not make influence over chain properties.

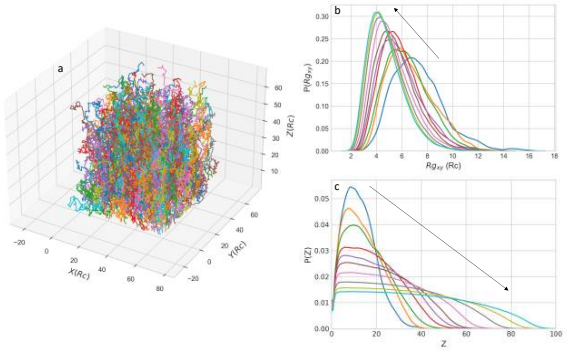

Figure 2. (a) snapshot of the equilibrated system with $N = 98$ and $\rho_s = 0.083 R_c^{-2}$ (b) radius of gyration and (c) brush height. Arrow indicates N growing from 10 to 98.

Our results show that excess chemical potential μ_{ex} presents a strong dependence of density surface ρ_s, degree of polymerization N, and excluded volume V_{ex} (Fig. 3). As we can see, μ_{ex} behaves as a linear function of ρ_s, increasing its slope as N increases, then applying log scale, one can see that it tends to reach a plateau for high ρ_s. For excluded volume V_{ex}, we observed that the effect is more pronounced for high dense systems $\rho_s > 0.14 R_c^{-2}$.

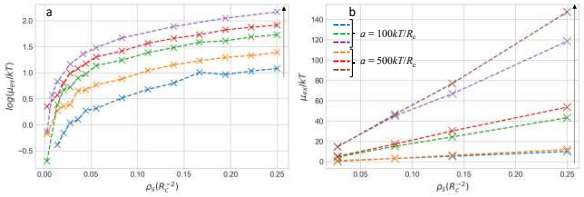

Figure 3: (a) excess chemical potential μ_{ex} dependence of surface density ρ_s for different chains lengths N (b) μ_{ex} dependence of excluded volume V_{ex} according to ρ_s and N ($N=10,40,98$). Arrow indicates N growing.

4. Conclusion

The modification of the expanded ensemble method allows a computational and an efficient exploration of the thermodynamics of polymer brushes. The data are being used to develop a scaling theory. Furthermore, the same methodology will be applied to surfactant adsorption and other strongly inhomogeneous systems with large complex molecules.

References

[1] Chen, W.L., Cordero, R., Tran, H., and Ober, C.K., 50th Anniversary Perspective: Polymer Brushes: Novel Surfaces for Future Materials, Macromolecules, 50(11), pp. 4089–4113, 2017.

[2] Binder, K. and Milchev, A., Polymer brushes on flat and curved surfaces: How computer simulations can help to test theories and to interpret experiments, J. Polym. Sci. B, 50(22), pp. 1515–1555, 2012.

[3] De Gennes, P.G., Scaling theory of polymer adsorption, J. Phys., 37(12), pp. 1445–1452, 1976.

[4] Widom, B., Some Topics in the Theory of Fluids, J. Chem. Phys., 39(11), pp. 2808–2812, 1963.

[5] Shing, K.S. and Gubbins, K.E., The chemical potential in dense fluids and fluid mixtures via computer simulation, Mol. Phys., 46(5), pp. 1109–1128, 1982.

[6] De Pablo, J.J., Laso, M., Ilja Siepmann, J., and Suter, U.W., Continuum-configurational-bias monte carlo simulations of long-chain alkanes, Mol. Phys., 80(1), pp. 55–63, 1993.

[7] Kumar, S.K., A modified real particle method for the calculation of the chemical potentials of molecular systems, J. Chem. Phys., 97(5), pp. 3550–3556, 1992.

[8] Lyubartsev, A.P., Martsinovski, A.A., Shevkunov, S.V., and Vorontsov-Velyaminov, P.N., New approach to Monte Carlo calculation of the free energy: Method of expanded ensembles, J. Chem. Phys., 96(3), pp. 1776–1783, 1992.

[9] Groot, R.D. and Warren, P.B., Dissipative particle dynamics: Bridging the gap between atomistic and mesoscopic simulation, J. Chem. Phys., 107(11), pp. 4423–4435, 1997.

[10] Zakharov I, et al: Zhores - Petaflops supercomputer for data-driven modeling, machine learning and artificial intelligence installed in Skolkovo Institute of Science and Technology, Open Engineering, 9(1), pp. 512-520, 2019.

Population contagion dynamics using active Brownian particles and probabilities of contagion as a model in computer simulations

Arturo Jimenez[1] **and Francisco Alarcon**[2*]
División de Ciencias e Ingenierías, Universidad de Guanajuato
Loma del Bosque 103, 37150 León, Mexico
[1] *ad.jimenezsalazar@ugto.mx*
[2] *paco@fisica.ugto.mx*

Abstract

One of the main difficulties faced by the whole world after the arrival of the Sars Cov-2 virus pandemic was the understanding of the virus itself, its physiology, the symptoms of the disease derived from the virus (COVID-19), but mainly its propagation due to the excessive growth of infected people around the world. Thus, understanding how the dynamics of contagion works has become a task of paramount importance in research and in the battle against the pandemic itself. In this project, we developed a model to study and understand the dynamics of contagion, different from classical statistical models such as the SI, giving greater degrees of freedom to potential parameters associated with contagion within the dynamics of infection, such as the spatial range of contagion, the use of masks, confinement of the population, etc. We have modeled the vulnerability of infection of a given individual as a probability to get infected. This method consists in the modelization of the population as active Brownian particles (ABP) on a fix area, such as a square, a classroom, etc. in order to describe the behavior of the infection and serve as a starting point for a better understanding of the spread of a virus. This methodology can serve as the scientific basis for the application of public policies and citizen protocols for the protection of the population. As well as the starting point for develop a software or application for the prevention of contagion.

Keywords: Infection, COVID-19, Active Brownian Particles, Mechanical Statistics, Numerical Simulations

1. Introduction

One of the most widely used techniques for modeling and predicting the growth of contagion is the SI (susceptibility to infection) model, which considers N agents that are either susceptible or infected individuals and a "contagion rate" these parameters establish a set of differential equations to model an infection curve, this model could include other population types, such as recovered, re-susceptible, etc. But the more parameters are added, the higher the complication to solve the equations.

We have try to understand the dynamics of the growth of contagion by using a model based on active Brownian particles. It is very well known that Brownian motion arose from the observations of Robert Brown (1773-1858) on a set of particles of a pollen grain in an aqueous environment with an unknown apparent reason for the motion dynamics of the pollen grain, thanks to the contributions of great scientific minds in the twentieth century it was deduced that these movements were caused by the water molecules that displaced the pollen particles, and that this movement could also be modeled, arriving at the Langevin equation and even what we know today as Brownian motion in the area of statistical mechanics.

Although the Brownian motion arises as an answer to a microscopic dynamics problem, its features can be used for macroscopic systems which, under some conditions and terms, can model agents walking on a square, but the Brownian motion is not enough, it needs a term of activity that allows the particles to move by themselves and not only by consequence of other particles or by their environment, this term would resemble the ability of people to walk and also another important point, which is the direction in which each of them would move, obtaining a model of what is known as "active matter" in this case, the model of active Brownian particles (ABP).

2. Contagion model

Given N particles that are moving in a squared box of size L with periodic boundary conditions and a self-propulsion force F_a for each particle (associated to the self-propel velocity), we model the contagion dynamics considering one "infected" at the beginning and the following contagion condition: if the distance between an "infected" and a "susceptible" particles is minor that a distance r_c, the "susceptible" will become infected.

Additionally, we have considered different suceptibilities with a contagion probability; if the distance between two "infected" and "susceptible" particles is minor that a contagion distance r_c then susceptible will become infected according to the probability of contagion p of the "susceptible" particle.

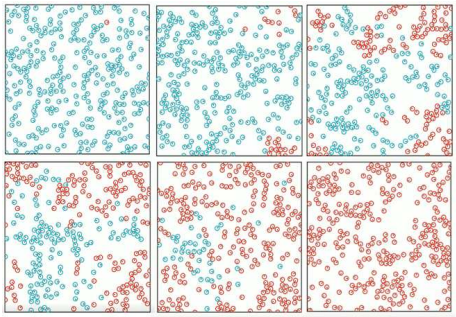

Figure 1: Footages taken at diferent times of a simulation with 300 particles in a squared box of size 34.32 with a self-propulsion force 80 in order to illustrate the dynamics of the simulation.

*F.A. acknowledges support from Apoyo a la Incorporación de Nuevos PTC del Programa para el Desarrollo Profesional Docente, Tipo Superior (PRODEP) 511-6/2020-8590.

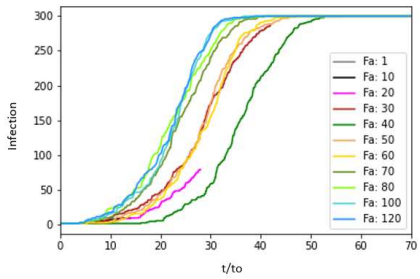

Figure 2: Previous results of simulations with 300 particles in a squared box of size 34.32 using different self-propulsion forces, were t/to is a normalization of the time based on stokes time for the particles

3. Conclusions

We will show preliminary results of our conditional model of contagion, taking in count the concentration of agents, de velocity of propulsion and the probability of contagion that can be associated to non-vaccinated agents or vaccinated agents with different dosis or vaccine brands.

References

[1] Martin-Roca, José, Raul Martinez, Lachlan C. Alexander, Angel Luis Diez, Dirk GAL Aarts, Francisco Alarcon, Jorge Ramírez, and Chantal Valeriani. "Characterization of MIPS in a suspension of repulsive active Brownian particles through dynamical features." The Journal of Chemical Physics 154, 16 (2021): 164901.

[2] Rodriguez, Diego Rogel, Francisco Alarcon, Raul Martinez, Jorge Ramírez, and Chantal Valeriani. "Phase behaviour and dynamical features of a two-dimensional binary mixture of active/passive spherical particles." Soft matter 16, 5 (2020): 1162- 1169.

[3] Norambuena, A., Valencia, F.J. and Guzmán-Lastra, F. "Understanding contagion dynamics through microscopic processes in active Brownian particles". Sci .Rep. 10, 20845 (2020). https://doi.org/10.1038/s41598-020-77860-y

[4] Zhao, Yinong, Cristián Huepe, and Pawel Romanczuk. "Contagion dynamics in self-organized systems of self-propelled agents." arXiv preprint arXiv:2103.12618 (2021).

Predicting the Phase Behavior of the Carbon Dioxide + Water from the SAFT-VR approach. The effect of the polar and quadrupolar interactions.

José Luis Ocaña[1], **Alejandro Martínez-Borquez**[2], **Víctor M. Trejos**[1*]

[1]*Instituto de Ciencias Básicas e Ingeniería, Universidad Autónoma del Estado de Hidalgo.*[2]*Escuela de Ingeniería y Ciencias, Tecnológico de Monterrey.*

Abstract

In this work we explore the phase behavior of carbon dioxide + water within the framework of the statistical associating fluid theory for potentials of variable range (SAFT-VR). The carbon dioxide molecule is modeled as two spherical segments tangentially bonded; the water molecule is modeled as a spherical segment with four associating sites which represent the hydrogen bonding. In both cases, the dispersive interactions are modeled using a square-well pair potential. The polar and quadrupolar interactions present in carbon dioxide and water are considered through an extension of the SAFT-VR approach that includes additional contributions to the Helmholtz free energy; lastly, the MX1a mixing rule is used for all the cases. The results show that the vapor-liquid phase diagram calculated with SAFT-VR approach are in good agreement with the experimental data taken from the literature in a wide range of thermodynamic conditions.

Keywords: SAFT-VR, mixture, quadrupolar

[*]Footnotes may appear on the first page only to indicate research grant, sponsoring agency, etc. These should not be numbered but referred to by symbols, e.g. *,+. The footnote text may be produced in a small font.

Rheological properties of the tear film lipid layer in health and disease

S. Jonguitud-Flores[1], Enrique O Graue-Hernández[2], Gabriel Espinosa[3], J. R. Vélez-Cordero[4]& Bernardo Yáñez-Soto[1].

[1]Laboratorio Nacional de Ingeniería de la MateriaFuera de Equilibrio.Instituto de Física"Manuel Sandoval Vallarta", Universidad Autónoma de San Luis Potosí. Manuel Nava 6, ZonaUniversitaria. C. P. 78290, San Luis Potosí. SLP, México. [2]Departamento de Córnea y CirugíaRefractiva, Instituto de OftalmologíaFundaciónConde de Valenciana IAP, Ciudad de México, México.

[3]Instituto de Física y Matemáticas, Universidad Michoacana de San Nicolás de Hidalgo, 58000 Morelia, Michoacán, México.
[4]Instituto de Física "Manuel Sandoval Vallarta", Universidad Autónoma de San Luis PotosíManuel Nava 6, ZonaUniversitaria. C.P. 78290, San Luis Potosí. SLP, México

Abstract
An essential component for vision is the eye surface, which is constituted by cells that cover up the expose area of the eye, lid margin, and the tear film. The tear film is a complex colloidal system, form by a mucin-gel layer, an aqueous layer and a lipid film on the outermost surface. The lipid film is composed mostly by meibomian gland lipids, and has a crucial role maintaining ocular surface homeostasis. Among its many functions it provides stability to the tear film and retards its evaporation, work as a barrier against foreign particles additionally has antimicrobial activity. These functions require the formation of a stable, continuous lipid layer to tolerate a range of different stresses. In this work we measured viscoelastic properties of meibomian gland lipids from both healthy people and patients suffering from meibomian gland diseases using a quartz crystal microbalance with dissipation and the Kelvin-Voigt model.

Keywords: Tear film lipid layer, meibomian gland lipids

*Corresponding author. Email address: silviajonguitud16@gmail.com

Self-diffusion coefficient and thermodynamic properties of the triangular-well fluid from Molecular Dynamics simulations.

Miriam de Jesús Sánchez[1], **Alexis Torres Carbajal**[2], **Víctor M. Trejos**[1*]

[1]*Instituto de Ciencias Básicas e Ingeniería, Universidad Autónoma del Estado de Hidalgo.*[2]*Unidad Profesional Interdisciplinaria de Ingeniería campus Tlaxcala, Instituto Politécnico Nacional.*

Abstract

In this work, we present a systematic study of the self-diffusion coefficient for a fluid of particles interacting via the triangular-well pair potential, determined by means of Molecular Dynamics simulations in the canonical (N, V, T) ensemble. The self-diffusion coefficient is determined for several fluid densities at supercritical thermodynamic states. The dependence of the self-diffusion coefficient on the potential range λ is analyzed in the range of $1.3 \leq \lambda \leq 2.6$. Aditionally, thermodynamic properties as the vapor-liquid coexistence, vapor pressure, internal energy, and critical properties are examined by using computer simulations. Simulation results are compared against the Barker-Henderson perturbation theory (BH PT). We observed a very good agreement between simulation results and the BH perturbation theory in a wide range of temperatures and pressures. Finally, the simulation data is used to model thermodynamic properties of real fluids as methane, fluoromethane hydrogen sulfide, and oxygen. These thermodynamic properties are in excellent agreement with the experimental data reported in the literature for a wide range of thermodynamic conditions.

Keywords: Self-diffusion coefficient, thermodynamic properties, triangular-well fluid, molecular dynamics.

[*]Footnotes may appear on the first page only to indicate research grant, sponsoring agency, etc. These should not be numbered but referred to by symbols, e.g. *,+. The footnote text may be produced in a small font.

Simulations of Active Brownian Particles in an Optical Trap

G.R. Vargas[1] *and **F. Alarcon**[2] †

[1] *Instituto de Física y Matemáticas, Universidad Michoacana de San Nicolas de Hidalgo, Edificio C-3, Ciudad Universitaria, 58040 Michoacán, México*
gonzalo.vargas@umich.mx

[2] *División de Ciencias e Ingenierías, Universidad de Guanajuato, Lomas del Bosque 103, 37150 León, Mexico.*
paco@fisica.ugto.mx

Abstract

In this work we have taken the model developed by Volpe in 2014 [1] and generalize it for the implementation of some localized electric field models, we have carried out different cases of active Brownian particles (ABP), from dilute to concentrate regimes and various self-propulsion speeds. We show cases with and without MIPS, we focus on how the properties of the systems are modified by the field and taking as reference systems the case without field.

Keywords: ABP, MIPS, active matter, brownian dynamics, optical traps

1. Introduction

From the earliest work done by Stenhammar [2] to the present day, a vast variety of models have been investigated which simulate dynamic systems of active particles Brownian particles, also known as ABP, the dynamics of this systems have been successfully simulated by evolving the Langevin equations in time [1]. Understanding the behavior of active Brownian particles can lead us to understand out-of-equilibrium systems such as some cases of bacteria among other examples [3]. ABP have different properties of great interest, such is the case of the formation of phase separation by motility (MIPS), this behavior has been studied and characterized under different fields [1, 4] or by varying the parameters of dynamics such as Péclet, Temperature, and packaging[5].

Within the variety of models that have been implemented, an important section has been dedicated to developed of models that reproduce the dynamics of colloidal systems have in the presence of electric fields [6]. Control over the propulsion direction and switchability of the interactions between the individual self-propelled units may open new avenues in designing of materials from within. Works of Volpe [7] and Vutukuri [8] reproduced the behavior of a molecule trapped in an optical trap and of the fusion and fission dynamics of switchable photoresponsive colloids, respectively, adding an external field to the Langevin equations.

In the following sections we present a development of the evolution with the finite difference method of the Langevin equations for Brownian systems with activity, the above based on the model of Volpe (2014). Subsequently, we introduce a localized electric field to analyze how the structural and orientational properties of the systems change, taking as a reference systems without an electric field.

2. Model

In the most general case, the 2D Langevin equations are:

$$\frac{d}{dt}\phi(t) = \sqrt{2D_R}W_\phi, \tag{1}$$

$$\frac{d}{dt}x(t) = \frac{D_T}{K_BT}(-\nabla_x U) + v\cos\phi(t) + \sqrt{2D_T}W_x, \tag{2}$$

$$\frac{d}{dt}y(t) = \frac{D_T}{K_BT}(-\nabla_y U) + v\sin\phi(t) + \sqrt{2D_T}W_y, \tag{3}$$

where ϕ the orientation of the particle, W represents an independent white noise process, while D_R and D_T are the rotational and translational diffusion respectively, U is the potential of interaction between two particles and v is the velocity of self-propulsion. The continuous solution of this set of stochastic equations can be approximated by a discrete-time sequence ($[\phi_i, x_i, y_i] \approx [\phi(t_i), x(t_i), y(t_i)]$) that is a solution of a finite difference equation of at regular time step ($t_i = it$). The numerical solution of equations 1-3 are

$$\phi_i = \phi_{i-1} + \sqrt{2D_R\Delta t}w_{\phi,i}, \tag{4}$$

$$x_i = x_{i-1} + \frac{D_T\Delta t}{K_BT}\sum_{j\neq i}(-\nabla_x U_{ij}) + v\cos\phi_i\Delta t + \sqrt{2D_T\Delta t}w_{x,i} \tag{5}$$

$$y_i = y_{i-1} + \frac{D_T\Delta t}{K_BT}\sum_{j\neq i}(-\nabla_y U_{ij}) + v\sin\phi_i\Delta t + \sqrt{2D_T\Delta t}w_{y,i}, \tag{6}$$

in these equations, w_i represents a random number from a normal distribution with mean zero and standard deviation equal to one, which is obtained by the box-Müller algorithm[9].

*G.R.V. acknowledges support provided by CONACYT for the development of this research.
†F.A. acknowledges support from Apoyo a la Incorporación de Nuevos PTC del Programa para el Desarrollo Profesional Docente, Tipo Superior (PRODEP) 511-6/2020-8590.

The main line of research focuses on the interaction potential between molecules (U), we use one of the most common to simulate the repulsive nature of ABP known as the WCA potential, whose equation is

$$U_1(\mathbf{r}_i, \mathbf{r}_j) = \begin{Bmatrix} 0, \text{for } r_{ij} > 2^{1/6}\sigma \\ 4\epsilon\left[\left(\frac{\sigma}{r_{ij}}\right)^{12} - \left(\frac{\sigma}{r_{ij}}\right)^{6} + \epsilon\right], \text{for } r_{ij} \leq 2^{1/6}\sigma \end{Bmatrix} \tag{7}$$

where σ is the radio of the particle, ϵ is the depth of potential and r_{ij} is the distance between two molecules.

The first approximation to simulate an optical trap make by Schmidt [6] was add an attractive interaction follow the Lennard-Jones potential scaled by a parameter ($\alpha << 1$) which determines the relative interaction strength among non-absorbing particles compared to the interaction strength among absorbing particles, therefore we can write the potential, when we turn on the optical trap, as follow:

$$U_2(\mathbf{r}_i, \mathbf{r}_j) = \begin{Bmatrix} 4\alpha\epsilon\left[\left(\frac{\sigma}{r_{ij}}\right)^{12} - \left(\frac{\sigma}{r_{ij}}\right)^{6}\right], \text{for } r_{ij} > \sigma \\ 4\epsilon\left[\left(\frac{\sigma}{r_{ij}}\right)^{12} - \left(\frac{\sigma}{r_{ij}}\right)^{6}\right], \text{for } r_{ij} \leq \sigma, \end{Bmatrix} \tag{8}$$

Finally, the general potential is the sum of the WCA potential and the potential proposed by Schmidt, that is $U = U_1 + U_2$.

3. Results

All the systems that were developed are dimensionless by set $K_BT = 1$, $\sigma = 1$, $\epsilon = 1$ and use the relations of Stokes-Einsten for the traslational and rotational diffusion [5]. The preliminary results of the configurations without optical trap (potential of equation 7) are shown in Fig. 1, we illustrate snapshots of the final state of six systems with two different packing fraction ($\phi \approx 0.43$ upper pictures and $\phi \approx 0.52$ bottom pictures), the images on the left have a velocity of self-propulsion of 0, the central ones of 50 and the images on the right of 100.

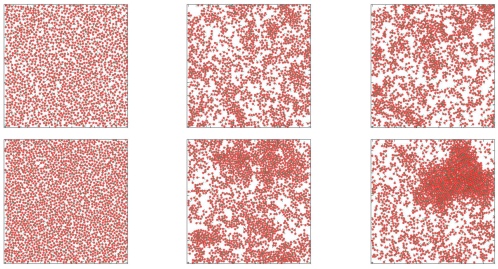

Figure 1: Snapshots of final configuration for systems with packing fraction of 0.43 (upper pictures) and 0.52 (down pictures), with different velocity of self-propulsion: 0 (left), 50 (center) and 100 (right).

Structurally, we can differentiate the formation of MIPS in the configuration corresponding to a packing fraction of 0.52 and a velocity of self-propulsion of 100, which is in agreement with the results shown in previous works. In subsequent sections we will analyze the mean square displacement and the density histogram to verify the configurations in which MIPS appear. Later, it will be shown how these properties are modified by changing the potential of equation 7 for the potential 8.

References

[1] VOLPE, G.; GIGAN, S. and VOLPE, G., Simulation of the active Brownian motion of a microswimmer, *American Journal of Physics*, vol. 82, no 7, p. 659-664, 2014.

[2] STENHAMMAR, Joakim, et al. Phase behaviour of active Brownian particles: the role of dimensionality. Soft matter, 2014, vol. 10, no 10, p. 1489-1499.

[3] ZHANG, He-Peng, et al. Collective motion and density fluctuations in bacterial colonies. Proceedings of the National Academy of Sciences, 2010, vol. 107, no 31, p. 13626-13630.

[4] FILY, Yaouen; HENKES, Silke; MARCHETTI, M. Cristina. Freezing and phase separation of self-propelled disks. Soft matter, 2014, vol. 10, no 13, p. 2132-2140.

[5] MARTIN-ROCA, José, et al. Characterization of MIPS in a suspension of repulsive active Brownian particles through dynamical features. The Journal of Chemical Physics, 2021, vol. 154, no 16, p. 164901.

[6] SCHMIDT, Falko, et al. Light-controlled assembly of active colloidal molecules. The Journal of chemical physics, 2019, vol. 150, no 9, p. 094905.

[7] VOLPE, Giorgio; VOLPE, Giovanni. Simulation of a Brownian particle in an optical trap. American Journal of Physics, 2013, vol. 81, no 3, p. 224-230.

[8] VUTUKURI, Hanumantha Rao, et al. Light-switchable propulsion of active particles with reversible interactions. Nature communications, 2020, vol. 11, no 1, p. 1-9.

[9] G. E. P. Box and Mervin E. Müller, A Note on the Generation of Random Normal Deviates, The Annals of Mathematical Statistics (1958), Vol. 29, No. 2 pp. 610-611

Single-trajectory analysis of droplets produced by spontaneous emulsification at water/glycerol/dodecane/span80 interface

M.J. Martínez-López[1,*] **and J.L. Arauz-Lara**[1]

[1] *Instituto de Física "Manuel Sandoval Vallarta", Universidad Autónoma de San Luis Potosí, Álvaro Obregón 64, 78000 San Luis Potosí, S.L.P., México*

Abstract

In order to study transport of droplets produced by spontaneous emulsification at an interface, the water/glycerol/ dodecane / span 80 system was analyzed. The experimental arrangement consisted of a rectangular stainless steel cell with two cylindrical concentric holes. The holes are perpendicular to the plane of the cell and water mixed with 1% (w/w) glycerol is placed in the upper hole, while dodecane mixed with 2% (w/w) Span 80 was placed in the lower hole. The emulsification process happens at the interface. In this configuration the interface is a concave meniscus, which in the observation region is considered as a plane because, the curvature radius of the meniscus is much larger than the cell radius. The presence of glycerol slows the droplets movement allowing, that in the observation region ($38.78\,\mu m \times 29\,\mu m$) trajectories of greater length to be obtained than those obtained without glycerol. We observed the interface using an inverted microscope (Olympus IX71) with a 50x (0.5 NA) objective. Due to the surfactant characteristics, we observed water/glycerol droplets in dodecane. The droplets slowly move towards the lowest point of the meniscus and form a colloidal crystal. We analyze the last colloidal crystal stage formation, as few drops are added. For this purpose, three observation regions are distinguished with respect to the colloidal crystal boundary: far, intermediate and near droplets. The recording times are about 120 seconds (with a ThorLabs camera, 22.9 *fps*), time in which it can be considered that the crystal boundary is approximately in the same place, because as the droplets grow over time the size of the colloidal crystal increases not only because of the new droplets are added but also because those already in place increase their volume causing the shift boundary. The droplets motion is a Brownian motion with drift. The velocity decreases as the droplets approach to the crystal boundary, where the droplets behave similar to approaching a wall. It is important to mention that each trajectory is unique, probably due to interface irregularities. For this reason, each trajectory was analyzed individually in its x and y coordinates, sectioning it where there was a change of direction and therefore velocity. For each trajectory fragment, the velocity and mean square displacement of each of the droplets were calculated. In order to verify the obtained results, we subtracted the velocity of each trajectory fragment to recover only the droplets Brownian behavior. Preliminarily, the results show that the density of probability histograms are equivalent for each region at different times. So the droplets behave similarly in equivalent regions at different times.

Keywords: Spontaneous emulsification, Water-oil interface, single-trajectory analysis

[*] Corresponding author. E-mail address: mariamtz@ifisica.uaslp.mx

The effect of masks and vaccination in the contagion dynamics by using active Brownian particles.

I.S. Regalado Alvarado[1] **and F. Alarcon**[2*]
División de Ciencias e Ingenierías, Universidad de Guanajuato
Loma del Bosque 103, 37150 León, Mexico
[1] *sicaru.regalado.alvarado@gmail.com*
[2] *paco@fisica.ugto.mx*

Abstract

The events from the last years have risen the interest in infection dynamics and models that can provide data to prevent more cases. Using active Brownian particles (ABP) as an alternative to statistical models such as the SI model to describe the infection dynamics.

We have carried out numerical simulations with N ABP particles, we have compared how does it affects in the contagion rate the introduction of N_p protected agents that are immune to the virus and cannot get infected. For a real situation, N_p would represent those individuals that had got vaccinated, wash their hands, wear protection such as facemasks, face shields, gloves, and so on.

The results can be used to increase awareness of the importance had has sticking to the protocols that inform us of the measures we can take to avoid getting infected.

Keywords: COVID, Active Brownian Particles, Mechanical Statistics, Numerical Simulations

[*]F.A. acknowledges support from Apoyo a la Incorporación de Nuevos PTC del Programa para el Desarrollo Profesional Docente, Tipo Superior (PRODEP) 511-6/2020-8590.

Transport properties of active Brownian particles in external periodic fields

Miguel A. Sandoval-Puentes[1], **Ramón Castañeda-Priego**[2] **and Francisco Alarcon**[3]
División de Ciencias e Ingenierías, Campus León, Universidad de Guanajuato
Loma del Bosque 103, 37150 León, Guanajuato, México
[1]*ma.sandovalpuentes@ugto.mx*
[2]*ramoncp@ugto.mx*
[3]*paco@fisica.ugto.mx*

Abstract

The structural and dynamical properties of colloidal active particles have attracted the interest of the scientific community in recent years. Interesting collective phenomena have been reported in experiments, theoretical approximations and computer simulations. Moreover, the motion of active particles in complex environments has gained the attention of recent physics researches because the novel phenomena that emerge, such as as trapping, sorting, clogging and also ratchet effects, mainly due to the disorder of the environment. In this work, by means of extensive Brownian dynamics computer simulations, a systematic analysis of the transport properties of a single active Brownian particle in an external periodic field has been performed . Our results point out on the existence of dynamical regimes that emerge due to the competition between the self-propulsion force and the strength of the external potential. Also, oscillatory behavior in the self-intermediate scattering function has been observed, as it is expected for pure active Brownian particles or another systems out of equilibrium, as in driven colloidal systems. The analysis of these oscillations and the effect of the external periodic field on the dynamical properties are explicitly discussed.

Keywords: Active Brownian particle, inhomogeneous landscape, transport properties

1. Introduction

Active matter is a novel class of nonequilibrium systems composed of self-propelled agents able to take up energy from their environment or from an internal source of energy, and converting it into directed motion [1, 2]. The motion of active particles in complex environments has attracted the attention of recent physics research because the non-trivial dynamics that take place, for instance, trapping, sorting, and clogging of particles. Examples of active matter systems embedded in complex environments are self-propelled particles in randomly disordered sites [3], periodic arrays of fixed obstacles [4] and external optical fields [5, 6]. A commonly used model to describe the movement of self-propelled colloids is the active Brownian motion. These Active Brownian Particles (ABPs) are modeled as self-propelled agents with constant velocity and direction of motion subjected to rotational diffusion and also with thermal diffusion. The equations of motion for a single ABP subjected to an external field can be written as,

$$\vec{r}(t+\Delta t) = \vec{r}(t)+\beta D_T \left(F^a \hat{u}(t) + \vec{F}^{pf}(t)\right) \Delta t + \delta\vec{R}^s(t), \quad (1)$$

where β is the Boltzmann factor and D_T the translational diffusion coefficient. The term F^a characterizes the self-propulsion force with orientation given by the unit vector $\hat{u}(t) = (\cos\phi(t), \sin\phi(t))$ and with $\phi(t+\Delta t) = \phi(t)+\delta\phi^s(t)$. $\vec{F}^{pf}(t)$ describes the coupling between the particle and the external field. The stochastic displacements, $\delta\vec{R}^s(t)$, and orientational fluctuations, $\delta\phi^s(t)$, follow a Gaussian-like distribution with zero mean and delta-correlated.
In this work, results from a systematic analysis using Eq. (1) focused mainly on the effect of the competition between the self-propulsion force and the confinement induced by an external periodic potential over the transport properties of an ABP (see Fig. 1) are presented. We have considered an external field with a one-dimensional periodicity and wavelength $\lambda = \sigma$, with σ being the ABP diameter.

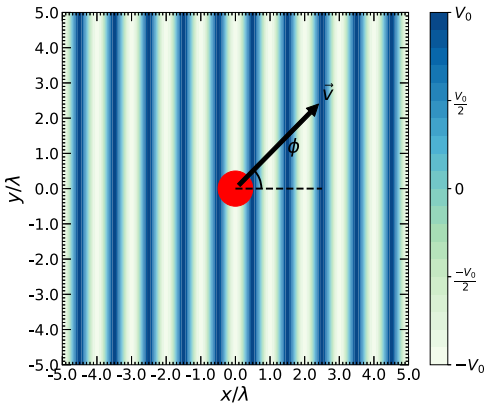

Figure 1: Schematic representation of an active Brownian particle with self-propulsion velocity $\vec{v}$ in an external potential with one-dimensional periodicity and strength V_0.

2. Mean square displacement

For an ABP in an inhomogeneous landscape, the competition between the confinement induced by the external field and the self-propulsion generates a rich dynamical behavior. Due to the geometrical form of the external field, its effect on the particle dynamics will be more evident in the mean square displacement at the perpendicular direction to the potential minima, namely $\langle\Delta x^2(t)\rangle$. In Fig. 2 a comparison of the $\langle\Delta x^2(t)\rangle$ for several self-propulsion forces given in terms of the adimensional Péclet

number, where $Pe = \frac{\sigma F_a}{K_B T}$, of an ABP in an external periodic field with strength $\beta V_0 = 20$ is displayed.

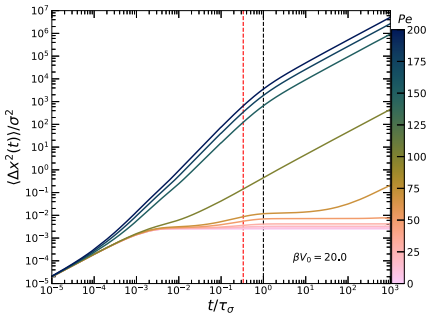

Figure 2: Mean square displacements, in the perpendicular direction to the potential minima $\langle \Delta x^2(t) \rangle$, of an active Brownian particle in an external field with strength $\beta V_0 = 20$. The color map is associated with the self-propulsion force (Péclet numbers).

For the most general case, it does appear a Brownian diffusion regime at short times followed by a subdiffusive dynamical behavior at intermediate times, linked with the confinement induced by the external periodic field. The ABP moves around the potential minima in a diffusive way during small times intervals, however, due to the external potential, the ABP cannot walk away so far from there. After that, at intermediate times $t < \tau_R$, a boost in the dynamics of the ABP is observed, associated with the self-propulsion force. When the orientation of the active force is pointing in the perpendicular direction to the potential fringes, the ABP achieves a bigger displacement around the minima, but remaining under confinement. This competition between the confinement induced by the harmonic field and the activity leads to a second plateau that appears at $t \approx \tau_\sigma$. When the self-propulsion is high enough to overcome the barrier, the particle can leave the potential minima. Eventually, the dynamics of the particle becomes again diffusive at long times.

3. Self intermediate scattering function

The self intermediate scattering function, $F_s(k,t)$ with $k = 2\pi/l$, constitutes the Fourier transform of the probability density of particle displacements. This function encodes a full statistical description about the particle behavior at a given length scale, l, and delay time, t, providing information about the correlation between particle positions along the time. In Fig. 3 a comparison of the $F_s(k,t)$ of an ABP in an external periodic field with strength $\beta V_0 = 20$, for several self-propulsion forces (Péclet numbers, Pe), considering $l = \sigma = \lambda$, is displayed. For low Pe values, the above-mentioned scattering functions decrease monotonically until reaching a constant value. However, as the activity increases, some oscillations in the $F_s(k,t)$ appear at intermediate times, $t \approx \tau_R$. Since these oscillations are present even in absence of external field (data not shown), they are completely associated with the self-propulsion of the ABP. Also, a damping in the amplitude of the oscillations is observed when the periodic potential is applied.

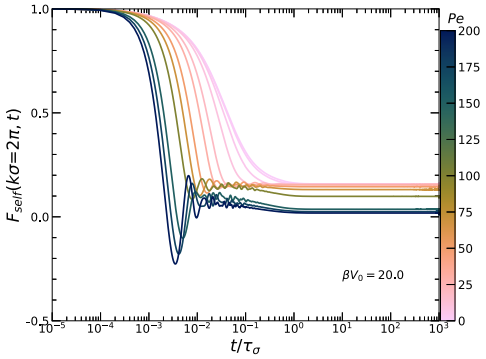

Figure 3: Self intermediate scattering functions for an active Brownian particle moving in an external periodic potential with strength $\beta V_0 = 20$. The colormap is associated with the self-propulsion force (Péclet number) of the ABP.

4. Concluding remarks

A systematic analysis of the transport properties of a single active Brownian particle moving in a complex environment was carried out. A completely rich dynamical behavior emerges due to the interplay between the self-propulsion force and the confinement induced by the external periodic potential. A manuscript with more detailed information will be submitted for publication [7].

5. Acknowledgements

The authors thankfully acknowledge computer resources, technical advise and support provided by Laboratorio Nacional de Supercómputo del Sureste de México (LNS), a member of the CONACYT network of national laboratories. Francisco Alarcon acknowledges support from Apoyo a la Incorporación de Nuevos PTC del Programa para el Desarrollo Profesional Docente, Tipo Superior (PRODEP) 511-6/2020-8590.

References

[1] Bechinger, C., Di Leonardo, R., Löwen, H., Reichhardt, C., Volpe, G. and Volpe, G., Active particles in complex and crowded environments, *Reviews of Modern Physics*, 88, p. 045006, 2016.

[2] Gompper, G., Winkler, R. G., Speck, T., Solon, A., Nardini, C., Peruani, F., Löwen, H., Golestanian, R. and Kaupp, U. B., Alvarez, L. and others, The 2020 motile active matter roadmap, *Journal of Physics: Condensed Matter*, 32, p.193001, 2020.

[3] Chepizhko, O., Franosch, T., Random motion of a circle microswimmer in a random environment, *New Journal of Physics*, 22, p. 073022, 2020.

[4] Reichhardt, C. and Reichhardt, C. J. O., Clogging, dynamics, and reentrant fluid for active matter on periodic substrates, *Physical Review E*, 103,p. 062603, 2021.

[5] McDermott, D. and Reichhardt, C. J. O. and Reichhardt, C., Collective ratchet effects and reversals for active matter particles on quasi-one-dimensional asymmetric substrates, *Soft Matter*, 12, pp. 8606–8615, 2016.

[6] Breoni, D., Schmiedeberg, M. and Löwen, H., Active Brownian and inertial particles in disordered environments: Short-time expansion of the mean-square displacement, *Physical Review E*, 102, p. 062604, 2020.

[7] Sandoval-Puentes, M. A., Castañeda-Priego, R. and Alarcón, F., Transport properties of Active Brownian particles in external periodic fields, *to be submitted*, 2021.

Viscoelastic properties for hard spheres colloidal system using SCGLE theory.

Orlando Joaquín Jaime [1] **Ricardo Peredo Ortiz**[1] **and Magdaleno Medina Noyola**[1]

[1] Instituto de Física "Manuel Sandoval Vallarta," Universidad Autónoma de San Luis Potosí,

Álvaro Obregón 64, 78000 San Luis Potosí, México

Abstract

Rheology is the science that studies the flow and deformation of matter. For the scientists who are in charge of studying this type of behavior, their greatest challenge has been to make theoretical predictions. Our main objective is to theoretically investigate properties such as shear viscosity $\Delta\eta(t)$ and the real and imaginary part of the dynamic viscosity $\eta(\omega)$, as well as the behavior of $\eta_{\infty}^{'}/\eta_0$, the derivation for the shear viscosity which derives the other properties was done differently from A. J. Banchio and G. Nagele[1], but the same result is reached using SCGLE theory [4]. These results are compared with A. J. Banchio and G. Nagele [1], Brownian Data simulation [2] and Chichoki and Federhof [3].

References

[1] G. Nägele and J. Bergenholtz, J. Chem. Phys. 108, 9893 (1998).

[2] P. Strating, Phys. Rev. E 59, 2175 (1999)

[3] B. Cichocki and B. U. Felderhof, Phys. Rev. A 43, 5405 (1991).

[4] L. Yeomans-Reyna and M. Medina-Noyola, Phys. Rev. E 64, 066114 (2001).

*Footnotes may appear on the first page only to indicate research grant, sponsoring agency, etc. These should not be numbered but referred to by symbols, e.g. *,+. The footnote text may be produced in a small font.

Waiting-time dependent non-equilibrium phase diagram of simple glass- and gel-forming liquids and states morphology

[1] Zepeda-López Jesús Benigno and Medina-Noyola Magdaleno

Abstract

This work proposes a solution to the problem of theoretically defining and predicting non-equilibrium phases and their time-evolving phase diagrams, of gel- and glass-forming materials. We demonstrate that these non-equilibrium phases and the corresponding non-stationary (i.e., aging) phase diagrams can indeed be defined and predicted using the kinetic perspective of a novel non-equilibrium statistical mechanical theory of irreversible processes. This is illustrated with the theoretical description of the transient process of dynamic arrest into non-equilibrium amorphous solid phases of an instantaneously quenched simple model fluid involving repulsive hard-sphere plus attractive square well pair interactions. In addition, an extension to the theoretical description can be made in order to describe the evolution of linear departures of density fluctuations. Such density fluctuations can be used to study the evolution of the system morphology across the resulting waiting-time dependent non-equilibrium phase diagrams, which allow us to determine and predict tendencies across these phase diagrams.

J. Chem. Phys. 154, 174901 (2021); doi: 10.1063/5.0039524

Keywords: NE-SCGLE theory, phase diagram, spinodal decomposition

1.

Unequal-Radius Modified Gouy-Chapman theory for the electrical double layer in several geometries

José Marcelo Padrón-Zamora[1], **Guillermo Iván Guerrero-García**[2], **Jonathan Josué Elisea-Espinoza**[1], **Enrique González-Tovar**[1*]

[1] *Instituto de Física "Manuel Sandoval Vallarta", Universidad Autónoma de San Luis Potosí,*

Álvaro Obregón 64, 78000, San Luis Potosí, SLP, Mexico
henry@ifisica.uaslp.mx

[2] *Facultad de Ciencias, Universidad Autónoma de San Luis Potosí*
Av. Parque Chapultepec 1570, 78210 San Luis, S.L.P., Mexico
givan@uaslp.mx

Abstract

In this work, we study the structural and electrostatic properties of the electrical double layer (EDL) in several geometries (planar, cylindrical, and spherical), for size- and charge-asymmetric electrolytes, via the URMGC theory. The integral equation version of the URMGC formalism is solved by using the Picard's Method. Notably, we report, for the first time, an analysis of the cylindrical EDL at the URMGC level. Our results corroborate the occurrence of the charge reversal (CR) and surface charge amplification (CA) phenomena. We investigate exhaustively the effect of the geometry on the EDL properties.

Keywords: electrical double layer, Poisson-Boltzmann theory, Gouy-Chapman theory

A numerical solution to the Poisson-Boltzmann differential equation for the electrical double layer via the Finite Element Method

Guillermo Guevara Zapata[1], **Guillermo Iván Guerrero García**[2], **Enrique González Tovar**[1]*

[1] *Instituto de Física "Manuel Sandoval Vallarta", Universidad Autónoma de San Luis Potosí,*

Álvaro Obregón 64, 78000, San Luis Potosí, SLP, Mexico
henry@ifisica.uaslp.mx

[2] *Facultad de Ciencias, Universidad Autónoma de San Luis Potosí*
Av. Parque Chapultepec 1570, 78210 San Luis, S.L.P., Mexico
givan@uaslp.mx

Abstract

We present a numerical solution to the Poisson-Boltzmann(PB) differential equation within the Finite ElementMethod (FEM) formalism. The PB equation describes the distribution of the electric potential in a solution referred to a charged solid in contact with an ionic solution, creating a layer of surface charges and counter-ions or electric double layer (EDL). The EDL, as a result of the variation of electric potential near a surface, has a significant influence on the behaviour of colloids and other surfaces in contact with solutions or solid-state fast ion conductors.

Keywords: electrical double layer, Poisson-Boltzmann theory, finite element method